Control of Chaotic Magnetic Fields in Tokamaks

I. L. Caldas [1], R. L. Viana [2], M. S. T. Araujo[1]*, A. Vannucci [1], E. C. da Silva [1], K. Ullmann [1], and M. V. A. P. Heller [1]

1. Instituto de Física, Universidade de São Paulo, C.P. 66318, 05315-970, São Paulo, São Paulo, Brazil.

2. Departamento de Física, Universidade Federal do Paraná, C.P. 19081, 81531-990, Curitiba, Paraná, Brazil.

Received on 2 April, 2002. Revised version received on 6 August, 2002.

Chaotic magnetic field lines play an important role in plasma confinement by tokamaks. They can either be generated in the plasma as a result of natural instabilities or artificially produced by external conductors, like resonant helical windings and ergodic magnetic limiters. This is a review of works carried out at the Universidade de São Paulo and Universidade Federal do Paraná on theoretical and experimental aspects of generation and control of chaotic magnetic field lines in tokamaks.

I Introduction

Chaotic behavior is one of the most intensively studied aspects of nonlinear dynamics, with applications ranging from physics to neuroscience, including virtually any branch of science and a great part of modern technology [1]. One of the areas in which chaotic dynamics has received most attention in recent past years is plasma physics. There are many reasons for this fact - if we consider a fluid model of a plasma, there are intrinsic nonlinearities in the model equations that may lead to complex behavior, as soliton propagation, intermittency, and turbulence [2,3]. These phenomena have been verified both in laboratory [4] and astrophysical plasmas [5]. In orbit theories, resonant particle-wave interactions have been considered as a paradigm for Hamiltonian chaos [6]. Charged particle motion in magnetic field configurations has been proved theoretically to give rise to chaotic dynamics, and has been related to ionospheric plasmas [7]. Three and four wave interactions is another subject in which nonlinear dynamics plays a major role [8], with many astrophysical applications [9].

In this paper we will focus on a specific type of plasmas, namely those generated and magnetically confined in fusion machines. For reasons that shall be clarified later on in this paper, chaotic dynamics is one of the striking properties of the magnetic field lines in tokamaks [10], stellarators [11], reversed field pinches [12,13] and other fusion machines; this has profound implications on the outcome of experiments. More specifically, we focus on the Lagrangian dynamics of the magnetic field line flow in tokamaks [14].

Tokamaks (a russian acronym for *toroidal magnetic chamber*) are toroidal pinches in which the plasma is formed by ohmic heating of a filling gas, produced by pulsed electric fields generated by transformer coils. The toroidal plasma is confined by the superposition of two basic magnetic fields: a toroidal field produced by coils mounted around the tokamak vessel, and a poloidal field generated by the plasma itself [15,16]. The superposition of these fields results in helical magnetic field lines. It is useful to consider these field lines as lying on nested toroidal surfaces, called magnetic surfaces, on which the pressure gradient that causes a plasma expansion is counterbalanced by the Lorentz force that appears due to the interaction between the plasma current and the magnetic field, in an equilibrium configuration [15,16]

This configuration is static, so that we describe the magnetic field lines in a Lagrangian fashion [14,17]. We parameterize the field lines by using a spatial ignorable coordinate (an azimuthal angle for axisymmetric configurations, like in tokamaks). This parameter plays the role of time, so that magnetic field line equations can be viewed as canonical equations; the other variables being field line coordinates and/or magnetic surface labels as well [18]. One of the advantages of this approach is the possibility of describing field lines by means of Hamiltonian maps, so reducing the number of degrees of freedom for the system [19]. In this framework, equilibrium configurations are integrable systems, whereas symmetry-breaking magnetic field perturbations spoil their integrability. This may lead to chaotic behavior, that in a Lagrangian sense

*Permanent Address: Universidade Cruzeiro do Sul, Av. Dr. Ussiel Cirilo 225, 08060-070, São Paulo, SP, Brazil

means that two initially nearby field lines diverge exponentially after many turns around a toroidal system [14,20]. However, if the chaotic field lines are trapped on small plasma regions, most of the lines can still be approximately described as they were averaged within the magnetic surface [21].

There are many situations in which the existence of chaotic magnetic field lines has deep implications for the plasma confinement in tokamaks. One is the control of the plasma-wall interactions, resulting from collisions of escaping plasma particles with the tokamak inner metallic wall [15], which is an important technological problem in the long-term operation of tokamaks [22]. The quality of the plasma confinement is affected by the presence of impurities released from the inner wall due to sputtering processes caused by localized energy and particle loadings. Controlling this interaction may lead to a decrease of the impurity content in the plasma core and an improvement of the plasma confinement. It is believed that chaotic magnetic field lines in the region next to the wall help to enhance heat and particle diffusion, so reducing localized attacks on the wall. Thus, to apply this effect, a device designed to create chaotic field lines in the plasma edge and near the wall, the ergodic magnetic limiter, was proposed to improve plasma confinement [23,24]. In fact, improvement of plasma confinement has been achieved by using ergodic magnetic limiters in several tokamaks [22,25,26].

Another application of chaotic magnetic field lines is related to the control of disruptive instabilities. Severe obstructions to the obtention of long lasting plasma confinement in tokamaks are due to these instabilities, which are usually preceded by Mirnov oscillations, or fluctuations of the poloidal magnetic field that can be detected by magnetic probes [27]. An experimental method to produce a chaotic region artificially uses conductors externally wound around the vessel wall in a suitable way, as resonant helical windings (RHW) [28,30,31]. These helical coils create resonant magnetic perturbations inside the plasma, in the same way ergodic limiters do in the plasma edge region. The use of RHW has been observed to inhibit these oscillations below a threshold value of the perturbation [28,30,31]. A RHW also creates a magnetic island structure within the plasma column that can be used to control magnetohydrodynamical (MHD) mode interaction. Thus, some type of disruptive instability can occur within this island structure, eventually leading to the loss of the plasma confinement. In this case, the existence of a thick layer of chaotic magnetic field lines may be considered the responsible for triggering these disruptions [28-30].

The localized creation of chaotic magnetic field lines in tokamaks, therefore, can be an important tool to investigate these instabilities, but care is needed to do so in a controlled manner, since a large scale chaotic region would simply destroy the plasma confinement. Control of chaotic magnetic field lines has been thus a major issue both of the experimental and theoretical tokamak research. Since the early 80's a research programme has been carried out at the Plasma Laboratory of the Instituto de Física - Universidade de São Paulo, Brazil, which has been systematically conducted in order to unveil the mechanisms whereby chaotic magnetic field lines in tokamaks may be created and, above all, controlled in a useful way. This programme has been pursued in close relation with the experimental group that built the first Brazilian tokamak, the TBR-1, as early as in 1978 [32]. The experimental and theoretical results obtained, involving the TBR-1 tokamak until the end of its operation in 1998, constitute an important Brazilian contribution to many areas of plasma physics. At present, a new machine, the TCABR [33], has replaced TBR-1 in the Plasma Laboratory of USP, and the control of chaotic field lines could be used in this machine as well [34].

The main purpose of this paper is to review part of the research program conducted at TBR-1, with emphasis on the mechanisms of generation and control of chaotic magnetic field lines by using ergodic magnetic limiters (EML) and resonant helical windings (RHW). We do not aim to review all the work published in the past twenty years or more by people that has worked in problems involving the TBR-1 but, instead, we focus on some contributions to the Hamiltonian description of field line flow, mentioning also other related work, whenever appropriate. In this spirit, we review some relevant experimental work carried out by TBR-1, mainly related to RHW and EML research, as well as plasma turbulence observations at the plasma edge.

The rest of this paper is organized as follows: in the next section we review some experimental results which we consider of relevance to the generation and control of chaotic field lines in tokamaks. In Section III a theory of integrable magnetic fields is presented, and in the following section the general Hamiltonian theory for almost-integrable fields is developed. Finally, Sections V and VI show the application of the theory to the cases of resonant helical windings and ergodic magnetic limiters, respectively. The last section is devoted to our conclusions.

II Experimental results

The basic geometry of a tokamak is depicted in Fig. 1, where we denote by b and R_0 the minor and major radius of the toroidal vessel respectively, so that the corresponding aspect ratio $A = R_0/b$ can be defined. The circular plasma column has a radius $a < b$. The poloidal and toroidal equilibrium magnetic fields point along the minor and the major curvatures along the torus, respectively. The resulting magnetic field line configuration is usually described by using some ap-

propriate coordinate system. The simplest of them is the cylindrical one: (R, Φ, Z), R being a radial coordinate with respect to the major axis, along which runs the Z coordinate [Fig. 1], and Φ is an azimuthal, or toroidal angle, usually an ignorable coordinate. The local coordinate system, depicted by Fig. 2, uses polar coordinates (r, θ) at a $\Phi = const.$ section of the torus, with the origin at the minor axis of the torus. The coordinate θ is commonly called the poloidal angle.

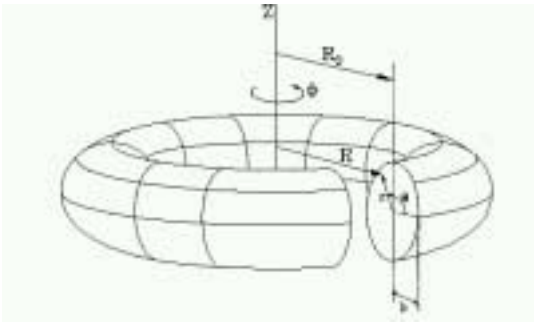

Figure 1. Schematic view of a tokamak.

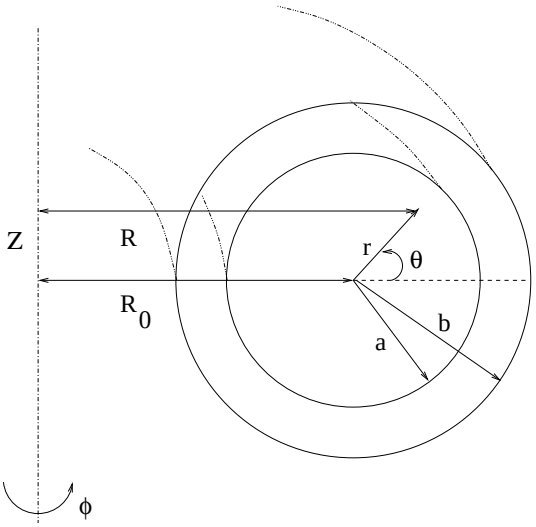

Figure 2. Cross section of a tokamak showing the relationship between cylindrical and pseudo-toroidal (local) coordinates.

The TBR-1 tokamak has its main parameters listed in Table I. Its ohmic heating transform and confining field coils were powered by capacitor banks. The vacuum vessel was made of stainless steel with eighteen access ports for diagnostic and pumping purposes. Base pressures of some microTorrs could be easily attainable by means of a turbomolecular pump. There were many standard diagnostics, like Mirnov coils, microwave interferometry, soft and hard X-rays, spectroscopy and electrostatic probes. Its assembly begun in 1977 and the first plasma, in tokamak mode, was obtained in 1980. Since the efforts of the Plasma Physics Laboratory of Instituto de Física were directed to the assembly of a new machine - the TCABR - the TBR-1 was disabled in 1998, as mentioned before.

Parameter	Symbol	Value
Major radius	R_0	0.30 m
Minor radius	b	0.11 m
Plasma radius	a	0.08 m
Toroidal field	B_0	0.5 T
Plasma current	$(I_P)_{max}$	12 kA
Central electron temperature	T_{e0}	200 eV
Central electron density	n_{e0}	$7 \times 10^{18} m^{-3}$
Pulse duration	τ_p	$7 - 9$ ms
Filling pressure	p	10^{-4} Torr

TABLE I: Main parameters of the TBR-1 tokamak [32].

During these more than twenty years of research, the TBR-1 machine had helped to develop a strong Brazilian experimental program in fusion plasmas along two main lines: (i) characterization and control of MHD activity, and (ii) study of plasma edge phenomena. In parallel with the experimental activities, a vigorous theoretical research program was conducted along the abovementioned lines. The main goal of this paper is to provide an overview of theoretical achievements in these areas. Before describing the theoretical framework on which this research is based, however, we shall present a brief summary of important experimental results, in order to give the reader a glimpse of the nature of the complex problems we usually find in fusion plasma theory.

The magnetohydrodynamical (MHD) plasma theory combines the continuum mechanics basic equations and constitutive relations with Maxwell's equations for a conducting fluid subjected to electric and magnetic fields [15,17]. While it is desirable to have a situation of global macroscopic MHD equilibrium to achieve magnetic plasma confinement, we have to be aware of the large number of macroscopic oscillations, or *MHD modes*, that may appear. The characterization and control of such MHD activity is a vital part of modern tokamak research. Thus, right from the beginning, the main MHD modes present in the TBR-1 discharges were experimentally identified [27].

The most important instabilities in tokamak plasmas are the disruptive instabilities. They are usually classified as internal (saw-teeth) and external, the latter being further subdivided into minor and major disruptive instabilities. The fingerprints of the major disruption, for example, are the presence of negative spikes in the loop voltage along the plasma, rapid loss of confined plasma energy, and an intense MHD activity with an explosive amplitude growth of the poloidal equilibrium field oscillations, which can be measured by the

Mirnov coils [28,30] leading, finally, to the total plasma collapse.

In the TBR-1 device there were added helical windings wound around the toroidal vessel whose function was to generate resonant MHD modes characterized by a wave vector $\mathbf{k} = (m/r)\hat{e}_\theta - (n/R_0)\hat{e}_\phi$ with a toroidal number $n = 1$ and the poloidal numbers $m = 2, 3, 4, \ldots$, depending on the combination chosen for the windings. The influence of these resonant helical currents on the Mirnov oscillations of TBR-1 discharges was first reported in Ref. [31]. Fig. 3 shows, for a typical TBR-1 discharge, the MHD activity represented by the behavior of the poloidal field oscillations $\tilde{B}_\theta$ when the current in the helical winding is activated. We see an attenuation of the Mirnov oscillation amplitude due to the action of the RHW with mode numbers $m : n = 2 : 1$. Interestingly, as soon as the external perturbing magnetic field ends, the MHD activity regains its original amplitude.

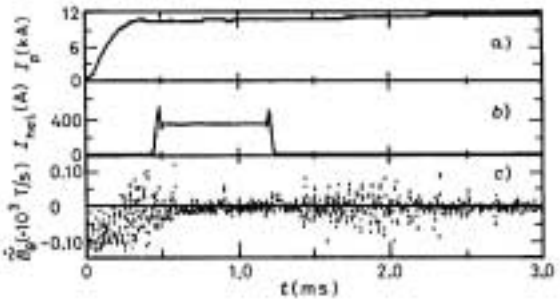

Figure 3. Time evolution of: (a) plasma current; (b) current in a 2/1 RHW; and (c) poloidal field oscillations during a discharge in TBR-1. Taken from Ref. [31].

The influence of RHW on the onset of the disruptive instabilities in the plasma discharges of the TBR-1 tokamak was also investigated in detail [29]. Fig. 4, for example, depicts the evolution of the plasma current in a controlled discharge with a series of minor disruptions before a major disruption takes place at $t \sim 1.5ms$. We show both the loop voltage spikes indicating the presence of minor disruptions and the consequent decrease of the MHD activity, as measured by the poloidal field (Mirnov) oscillations.

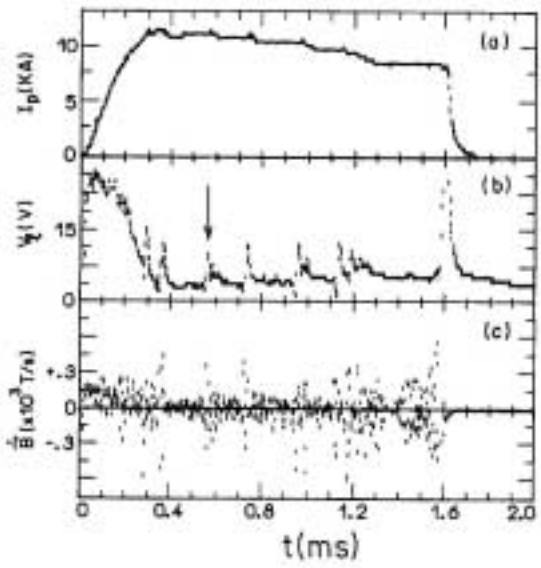

Figure 4. Time evolution of: (a) plasma current; (b) loop voltage, and (c) poloidal field oscillation during a discharge in TBR-1. The arrow in (b) indicates the occurence of a minor disruption. Adapted from Ref. [29].

A Fourier analysis of the oscillations showed that the dominant MHD modes involved in the precursor phase of the minor disruption for this discharge were the $m : n = 2 : 1$ and $3 : 1$ ones. Accordingly, a numerically obtained Poincaré map of magnetic field lines [Fig. 5], with the same parameters used in the experiment, has shown that the overlap of the corresponding magnetic islands plays a role in this process due to the existence of a chaotic magnetic field line region between the islands, which gives rise to a partial relaxation of the plasma discharge.

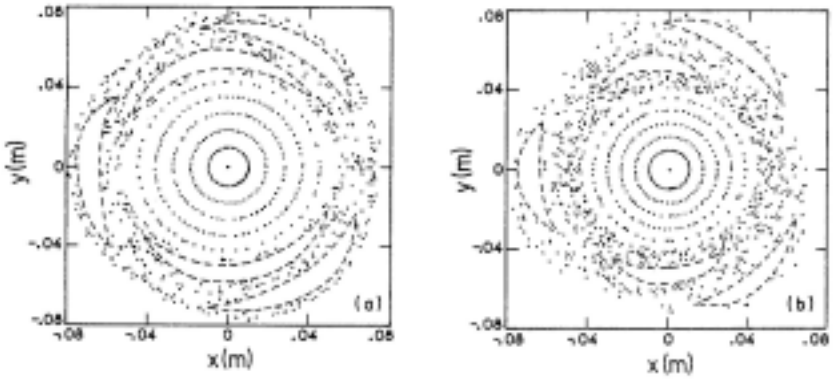

Figure 5. Intersections of magnetic field lines with a Poincaré surface of section $50\mu s$ (a) and at the instant (b) of the minor disruption indicated in Fig. 4. Taken from Ref. [29].

The knowledge of the transport properties of the plasma in the tokamak edge (i.e., the region comprising the outer portion of the plasma column and the vacuum region that separates it from the vessel wall) is essential to the stable operation of the tokamak [35,36]. Field line chaos plays here a major role in the interpretation of the experimental results, since it was long recognized that turbulent transport is particularly important in the plasma edge. A number of probes have been developed by the TBR-1 team to measure the particle density and temperature fluctuations in this region, as well as the particle confinement time [37]. The experimental results suggest that the turbulent transport is mainly of electrostatic nature [38]. These results have been also observed by analyzing data from other Tokamaks [39].

In spite of this, there have been performed studies on the correlation between electrostatic and magnetic fluctuations. It is believed that high-frequency MHD activity modulates the density and potential fluctuations in the plasma edge. Furthermore, the connection between turbulent density fluctuations and low-dimensional chaotic dynamics has been quantitatively verified by using suitable numerical algorithms like the correlation dimension [40] and the statistical distribution of recurrence times [41].

The influence of resonant magnetic perturbation caused by helical windings on the plasma edge parameters was studied by Caldas *et al.* [42]. The radial particle flux was found to be proportional to the density gradient at the plasma edge. In Fig. 6 the particle flux is plotted against the frequency, both with and without the action of the resonant helical windings. We see that a significative effect was produced due to the external resonant perturbation, showing not only a reduction of the particle flux throughout the spectrum, but also an inversion of the flux for some low frequencies.

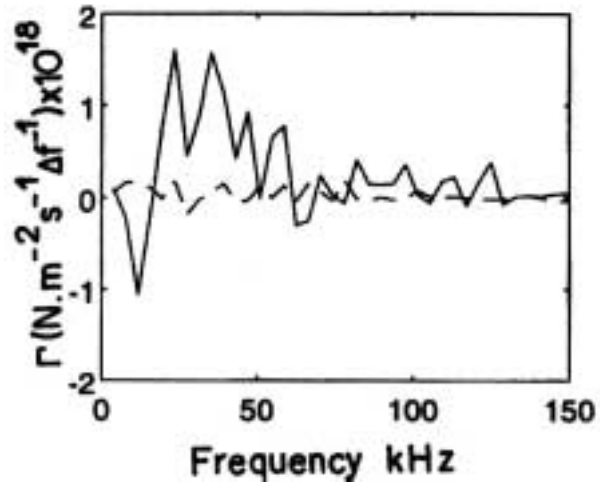

Figure 6. Particle flux spectrum at a fixed radial position $r = 0.89a$. Full and dashed lines indicate absence and presence of RHW action, respectively. Taken from Ref. [42].

In the TBR-1 tokamak, afterwards, the helical windings were replaced by an ergodic magnetic limiter (EML) composed of four poloidal rings, distributed along the toroidal directions, with toroidal and poloidal numbers $n = 2$ and $n = 7$, respectively. For several similar plasma discharges, both the mean electron density (Fig. 7) and electron temperature (Fig. 8) profiles were measured within the plasma edge with a triple electrostatic probe. As observed in Figs. 7 and 8, the experimental measurements show a decrease in temperature and density values, when the external perturbation is applied [43]. This indicates that more peaked profiles, and consequently a better confinement, can be obtained by means of an ergodic magnetic limiter.

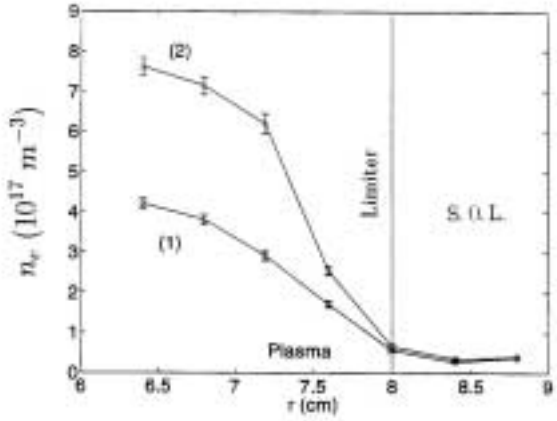

Figure 7. Radial profile of the mean electron plasma density with (2) and without (1) the action of an ergodic magnetic limiter. Taken from Ref. [43].

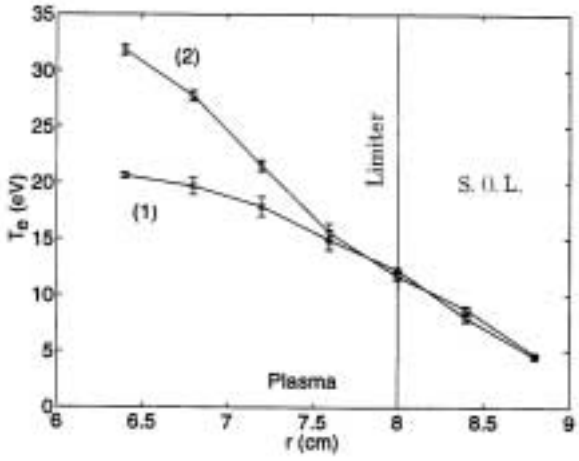

Figure 8. Radial profile of the electron plasma temperature with (2) and without (1) the action of an ergodic magnetic limiter. Taken from Ref. [43].

In relation to the possible use of an EML for controlling the disruptive instabilities, Fig. 9 shows the power

spectrum obtained prior (Fig. 9a) and just after (Fig. 9b) the EML is turned on [43]. As a result of the perturbing external field, the intensity of the MHD activity decreases, the MHD mode decomposition broadens up, and the corresponding mode frequency spectra are considerably enlarged, indicating that the ergodic limiter can indeed make the plasma confinement more stable [28,30].

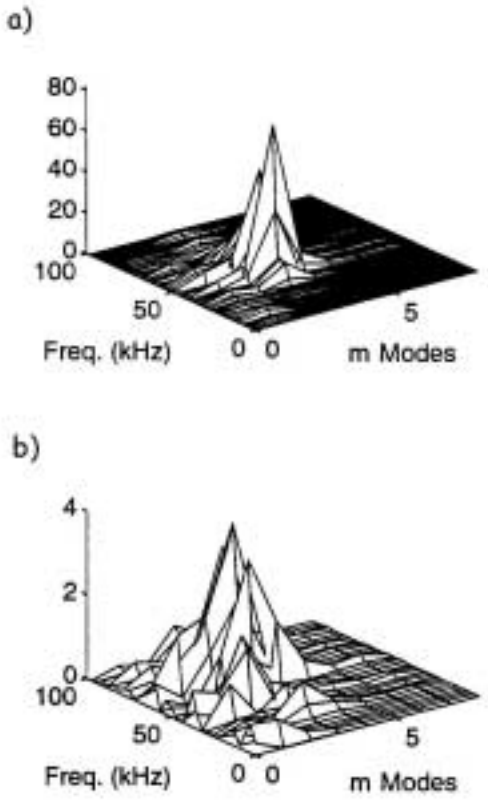

Figure 9. Power spectral densities *versus* the frequency and mode numbers, prior (a) and just after (b) an ergodic magnetic limiter is turned on. Taken from Ref. [43].

In summary, the effect of chaotic magnetic field lines, both within the plasma and at its edge, can not be overlooked when considering a variety of experimental phenomena related to MHD activity and edge transport. Hence, we need theoretical tools for describing the behavior of chaotic field lines in tokamak plasmas. This knowledge can be crucial for controlling the plasma stability when chaos is not desired or else for enhancing its effect when it turns out to be useful.

III Theory of integrable magnetic fields

The starting point of our theoretical treatment of plasma confinement in tokamaks is the equilibrium configuration, in which the velocity and all time derivatives vanish. The equilibrium magnetic field represents, in terms of the Hamiltonian description for field line flow, an integrable dynamical system. In this section we will review the basic equations of the MHD static equilibrium theory for axisymmetric plasmas and how they can be used to obtain the magnetic fields that confine the plasma in terms of the plasma characteristic parameters.

In the framework of MHD equilibrium theory, a necessary condition for plasma confinement is that the expansion caused by a pressure gradient must be counterbalanced by the Lorentz force produced by the plasma current density $\mathbf{J}_0 = (1/\mu_0)\nabla \times \mathbf{B}_0$, hence

$$\mathbf{J}_0 \times \mathbf{B}_0 = \nabla p_0, \tag{1}$$

where $\mathbf{J}_0$, $\mathbf{B}_0$ and p_0 are the plasma equilibrium electric current density, magnetic field and kinetic pressure, respectively. Taking the scalar product of (1) with the magnetic field results in

$$\mathbf{B}_0.\nabla p_0 = 0, \tag{2}$$

in such a way that the equilibrium magnetic field lines lie on constant pressure surfaces, or *magnetic surfaces.*

The pressure is an example of a surface quantity, i.e., some property that is constant on all points of a magnetic surface. Other important surface quantity is the *poloidal magnetic flux* Ψ_p, so that the condition (2) is equivalent to

$$\mathbf{B}_0.\nabla \Psi_p = 0. \tag{3}$$

and the magnetic surfaces are also *flux surfaces* characterized by $\Psi_p = const.$ [15,16]. Applying the same definition to the flux of current density lines, the *poloidal current flux* I is another surface quantity of interest.

The condition (1) is not sufficient for plasma confinement since, in addition to it, we must have *closed* magnetic surfaces. Using topological arguments we conclude that the plasma shall present azimuthal symmetry in order to have closed surfaces with the topology of nested tori. As a consequence, no surface quantity depends on the toroidal angle Φ. In the following subsections we shall discuss the equilibrium plasma configuration by using two coordinate systems.

When the confined plasma has some symmetry with respect to a given coordinate, it is possible to write the magnetic field line equations, $\mathbf{B}_0 \times \mathbf{dl} = \mathbf{0}$, in the form of Hamilton's equations of motion. We are considering static equilibrium situations, so the role of time is now played by the ignorable, or cyclic, coordinate. The remaining coordinates give the canonical position and momentum variables. The advantage of this procedure is that one can use the powerful methods of Hamiltonian dynamics, like perturbation theory, KAM theory, adiabatic invariance, etc. to analyze magnetic field topology when a static magnetic perturbation is applied on a given equilibrium field [6,44].

A Hamiltonian description for field line flow was first proposed by Kerst [46], and later used to describe the effect of non-symmetric perturbations in various plasma confinement machines: stellarators [47], levitrons [48] and tokamaks [10,49]. A Hamiltonian description valid in an arbitrary curvilinear coordinate system is also available [18]. and it has been applied for magnetic fields with helical symmetry [50] and spherical symmetry [51,52], the latter being relevant for some compact tori models (spheromaks and field reversed configurations).

A. Equilibrium in local coordinates

The local coordinate system (r, θ, φ) is a kind of "toroidalized" cylindrical system, in which the variable $z = R_0\varphi$ runs along the symmetry axis of the tokamak, where R_0 is its major radius and $\varphi = \Phi$ is the toroidal angle. This is a very simple and, as we shall see, sometimes unsatisfactory description, but it is able to describe situations in which the toroidal curvature does not play a major role. The flux surfaces are cylinders, for which $f(r) = const.$, where $f(r)$ is any smooth function of the surface radius. The magnetic axis is a degenerate surface with $r = 0$ [15,16].

A magnetic field which is consistent with the MHD equilibrium requirements is $\mathbf{B}_0 = (0, B_\theta(r), B_\varphi(r,\theta))$, where the poloidal field is obtained, through an application of Ampére's law, from a plasma current density whose radial profile is known, like the *peaked model* [53]

$$\mathbf{J}_\varphi(r) = \frac{I_p R_0(\gamma+1)}{\pi a^2}\left[1-\left(\frac{r}{a}\right)^2\right]^\gamma \hat{e}_\varphi, \qquad (4)$$

where I_p is the total plasma current, a is the plasma radius, and γ is a fitting parameter.

The toroidal field B_φ is either considered to be uniform (B_0) or, more precisely, a uniform component with a toroidal correction in the form

$$B_{0\varphi} = \frac{B_0}{1+\frac{r}{R_0}\cos\theta}, \qquad (5)$$

which takes into account that the toroidal field is higher in the inner portion of the torus [54].

The magnetic field lines satisfy the differential equations

$$\mathbf{B}_0 \times \mathbf{dl} = \mathbf{0}, \qquad (6)$$

and they wind on the cylindrical flux surfaces with a well-defined pitch related to the so-called *rotational transform* ι, which is the average poloidal angle swept by a field line after one complete toroidal turn. Mathematically it is given by [55]

$$\iota(r) \equiv 2\pi\frac{d\theta}{d\varphi} \equiv \frac{2\pi}{q(r)}, \qquad (7)$$

where q is the *safety factor* of the flux surface. The name safety factor comes due to the requirement that $q \geq 1$ on the magnetic axis to avoid kink instabilities that are dangerous to the plasma confinement (Kruskal-Shafranov criterion) [15]. Fig. 10 shows the radial profiles for the normalized plasma current density $J_\phi/J_{\phi 0}$ (10 a), poloidal field $B_\theta/B_{\theta a}$ (10 b), and rotational transform ι/ι_a (10 c). Tokamak parameters were taken from the TBR-1 machine (see Table I), and we set $q(r=0) = 1$ and $q_a = q(r=a) = 5$ at the magnetic axis and plasma edge, respectively.

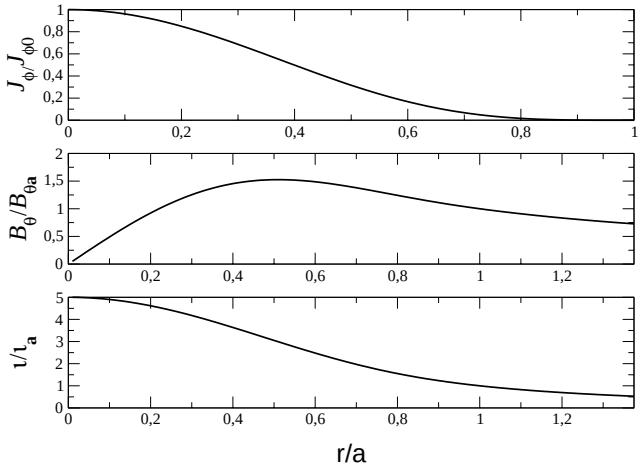

Figure 10. Radial profiles of the normalized (a) current density; (b) poloidal field; and (c) rotational transform for the model in local coordinates. Parameters were taken from Table I.

The Hamiltonian description of the field line flow in this case uses the following action and angle variables: $J = r^2/2$ and $\vartheta = \theta$, respectively, whereas the azimuthal angle $t = \varphi$ plays the role of time [56]. The magnetic field line equations can be written in a canonical form

$$\frac{dJ}{dt} = -\frac{\partial H_0}{\partial \theta}, \qquad (8)$$

$$\frac{d\theta}{dt} = \frac{\partial H_0}{\partial J}, \qquad (9)$$

referring to a Hamiltonian [57]

$$H_0(J) = \frac{1}{2\pi}\int_0^J \iota(J')dJ', \qquad (10)$$

In the case for which γ is an integer it is possible to write down an explicit form for this Hamiltonian [58]

$$H_0(J) = \sum_{k=1}^{\gamma+1} c_k(\gamma)\left(\frac{J}{J_a}\right)^k, \qquad (11)$$

in which $J_a = a^2/2$ and the coefficients are

$$c_k(\gamma) = \frac{J_a}{q_a}\frac{(-1)^{k+1}}{k}\frac{(\gamma+1)!}{k!(\gamma+1-k)!}. \qquad (12)$$

B. Equilibrium in polar toroidal coordinates

It is a common practice in mathematical physics to choose coordinate systems which reflects the symmetry of the system or the boundary conditions. The local coordinates (r, θ, φ) have the shortcoming that the coordinate surfaces $r = const.$ hardly coincide with actual equilibrium flux surfaces. This has led to a quest for more sophisticated systems, like the toroidal coordinates (ξ, ω, φ), that have been extensively used in spite of another drawback: their coordinate surfaces do not have the right Shafranov shift. The Shafranov shift is the outward displacement of the magnetic axis (a degenerate flux surface) with respect to the geometric axis, due to the toroidal geometry.

In order to overcome this problem, Kucinski and Caldas have introduced a polar toroidal coordinate system $(r_t, \theta_t, \varphi_t)$ [60] which, in the large aspect ratio limit, reduces to the local coordinate system and has the right Shafranov shift $R_0' - R_0$, where R_0' is the major radius of the magnetic axis. Further details about this coordinate system are found in the Appendix.

A MHD equilibrium theory of an axisymmetric plasma may be constructed upon the surface quantities like $\mathbf{J}$, $\mathbf{B}$ and p, or equivalently, on the surface quantities Ψ_p and I. The ideal MHD equations can be used to derive an elliptic partial differential equation for the poloidal fluxes, the so-called Grad-Shafranov-Schlüter equation [16]. It is written , in the polar toroidal system, as [61]

$$\frac{1}{r_t}\frac{\partial}{\partial r_t}\left(r_t\frac{\partial \Psi_p}{\partial r_t}\right) + \frac{1}{r_t^2}\frac{\partial^2 \Psi_p}{\partial \theta_t^2} = \mu_0 J_{30}(\Psi_p) + \mu_0 {R_0'}^2 \frac{dp_0}{d\Psi_p}\left(2\frac{r_t}{R_0'}\cos\theta_t + \frac{r_t^2}{{R_0'}^2}\sin^2\theta_t\right) + \\ + \frac{r_t}{R_0'}\left[\cos\theta_t\left(2\frac{\partial^2 \Psi_p}{\partial r_t^2} + \frac{1}{r_t}\frac{\partial \Psi_p}{\partial r_t}\right) + \sin\theta_t\left(\frac{1}{r_t^2}\frac{\partial \Psi_p}{\partial \theta_t} - \frac{2}{r_t}\frac{\partial^2 \Psi_p}{\partial \theta_t \partial r_t}\right)\right], \tag{13}$$

where J_{30} is the toroidal component of the equilibrium plasma current density, given by

$$J_{30}(\Psi_p) = -{R_0'}^2 \frac{dp_0}{d\Psi_p} - \frac{d}{d\Psi_p}\left(\frac{1}{2}\mu_0 I^2\right). \tag{14}$$

The relationships between the magnetic field contravariant components and the surface quantities Ψ_p and I are

$$B_0{}^1 = -\frac{1}{R_0' r_t}\frac{\partial \Psi_p}{\partial \theta_t}, \tag{15}$$

$$B_0{}^2 = \frac{1}{R_0' r_t}\frac{\partial \Psi_p}{\partial r_t}, \tag{16}$$

$$B_0{}^3 = -\frac{\mu_0 I}{R^2}, \tag{17}$$

where

$$R^2 = {R'}_0^2\left[1 - 2\left(\frac{r_t}{R'_0}\right)\cos\theta_t - \left(\frac{r_t}{R'_0}\right)^2\sin^2\theta_t\right]. \tag{18}$$

Analytical solutions to the Grad-Shafranov-Schlüter equation are rare, even for simple coordinate systems. We thus look for approximate solutions of (13) in the form $\Psi_p = \Psi_{p0}(r_t) + \delta\Psi_p(r_t, \theta_t)$, where $|\delta\Psi_p| \ll |\Psi_{p0}|$, and expand J_{30} and $dp_0/d\Psi_p$ in powers of $\delta\Psi_p$. In the large aspect ratio limit ($R'_0 \gg b_t$), and supposing that in lowest order the solution Ψ_{p0} does not depend on θ_t, Eq. (13) reduces to an unidimensional equation, similar to the one obtained in cylindrical coordinates. However, in our solution the intersections of the flux surfaces $\Psi_{p0}(r_t) = const.$ with a toroidal plane $\varphi = 0$ are not concentric circles and present a Shafranov shift toward the exterior equatorial region.

To solve the Grad-Shafranov-Schlüter equation we need, in addition, to assume spatial profiles for both the surface quantities p and I. In lowest order, however, it suffices to assume a single profile for J_{30}, as given by Eq. (14) in terms of p and I. So, we choose the peaked model [Eq. (4)]. We skip the details of the calculation, which may be found in Ref. [62]. In lowest order, the equilibrium field components are

$$B_0{}^1 = 0, \tag{19}$$

$$B_0{}^2(r_t) = B_a\left[1 - \left(1 - \frac{r_t^2}{a^2}\right)^{\gamma+1}\right], \tag{20}$$

$$B_0{}^3(r_t, \theta_t) = B_T\left(1 - 2\frac{r_t}{R_0'}\cos\theta_t\right)^{-1}. \tag{21}$$

where $B_a \equiv B_0^2(r_t = a) = \mu_0 I_p/2\pi r_t^2$, $B_T \equiv B_0^3(r_t = 0) = \mu_0 I_e/2\pi {R_0'}^2$, and $I_e \approx -I/2\pi$ for large aspect ratio.

The poloidally-averaged safety factor of the magnetic field lines is, in these coordinates, given by

$$q = q_c(r_t)\left(1 - 4\frac{r_t^2}{{R_0'}^2}\right)^{-1/2}, \qquad (22)$$

where

$$q_c(r_t) = \frac{I_e}{I_p}\frac{r_t^2}{{R_0'}^2}\left[1 - \left(1 - \frac{r_t^2}{a^2}\right)^{\gamma+1}\right]^{-1}. \qquad (23)$$

Figure 11 is a cross-section of the flux surfaces in a tokamak whose lengths are normalized to the minor radius ($b_t = 1$), and parameters are taken from Table I, such that: $a/R_0' = 0.26$, $q \approx 1$ at the magnetic axis and $q_a \approx 5$ at plasma edge ($r_t = a$). The zeroth and first order results practically coincide. Radial profiles for the poloidal $B_0^2(r_t)$ and toroidal $< B_0^3(r_t) >_{\theta_t}$ field components are depicted in Figs. 12 (a) and (b), respectively. The poloidal field is asymmetric with respect to the geometric axis, and the toroidal field is stronger in the internal part of the torus, since the coils that generate it are more densely packed there. Fig. 12 (c) shows the safety factor $q(r_t)$ profiles, and the difference between zero and first order results is noticeable only near the plasma edge and results in a slight displacement of the magnetic surfaces.

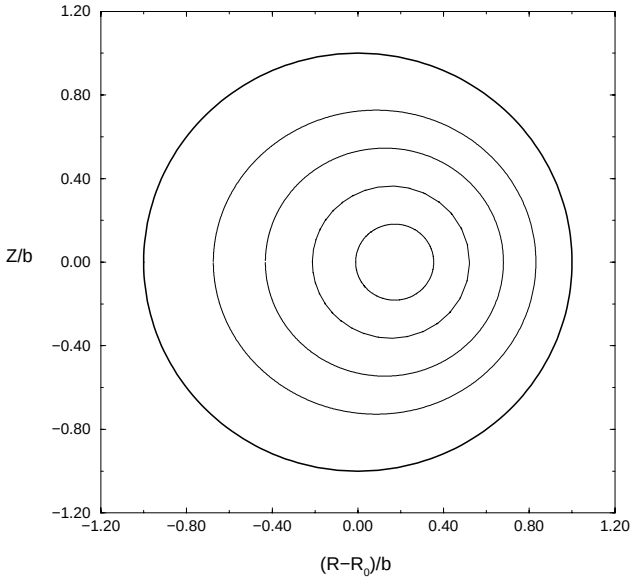

Figure 11. Flux surfaces for the MHD equilibrium model in polar toroidal coordinates. Parameters were taken from Table I.

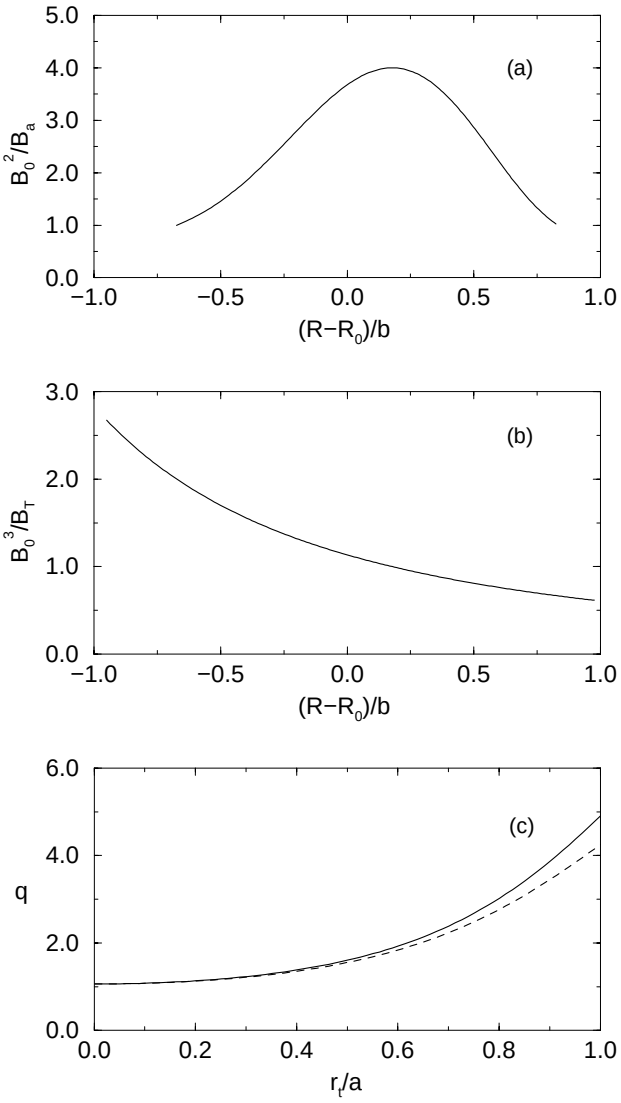

Figure 12. (a) Poloidal and (b) toroidal equilibrium magnetic field components; (c) safety factor of magnetic surfaces. Zeroth and first order results are shown by dashed and full lines, respectively.

In order to obtain a Hamiltonian formulation for field line flow in polar toroidal coordinates we shall define convenient action and angle variables. The action is defined in terms of the toroidal magnetic flux as [62]

$$\begin{aligned} J(r_t) &= \frac{1}{2\pi {R_0'}^2 B_T}\int \mathbf{B}_0.\mathbf{d}\sigma_3 \\ &= \frac{1}{4}\left[1 - \left(1 - 4\frac{r_t^2}{{R_0'}^2}\right)^{1/2}\right], \end{aligned} \qquad (24)$$

where $\mathbf{d}\sigma_3 = {R'}_0 r_t dr_t d\theta_t \hat{e}^3$. Expanding this action in powers of the aspect ratio gives, for the lowest order, the variable $r_t^2/2$, as in the previous section. The time-like variable will be the ignorable coordinate $t = \varphi_t$,

and the angle variable is a modified poloidal angle [63]

$$\vartheta(r_t,\theta_t) = \frac{1}{q(r_t)}\int_0^{\theta_t}\frac{B_0^3(r_t,\theta_t)}{B_0^2(r_t,\theta_t)}d\theta = 2\arctan\left[\frac{1}{\Omega(r_t)}\left(\frac{\sin\theta_t}{1+\cos\theta_t}\right)\right], \quad (25)$$

and the field line equations become Hamilton equations

$$\frac{dJ}{dt} = -\frac{\partial H}{\partial\vartheta}, \quad (26)$$

$$\frac{d\vartheta}{dt} = \frac{\partial H}{\partial J}, \quad (27)$$

with the integrable Hamiltonian

$$H = H_0(J) = \frac{1}{B_T R_0'^2}\Psi_{p0}(J), \quad (28)$$

where $B_T = \mu_0 I_e/2\pi R'_0$ is the toroidal field on the magnetic axis.

IV Theory of almost-integrable magnetic fields

Any magnetostatic field that breaks the exact axisymmetry of the equilibrium tokamak field is a non-integrable perturbation, from the Hamiltonian point of view. If the strength of these perturbations is not too high, it is possible to use standard results of Hamiltonian dynamics - like KAM theory, adiabatic and secular perturbation theory, etc. - to predict the behavior of the field lines in the presence of such *almost-integrable* magnetic fields. Two sources of perturbing fields shall be dealt with in this paper: resonant helical windings (RHW) and ergodic magnetic limiters (EML). Both examples can be treated using the same theoretical framework, that is the canonical perturbation theory, the difference being the dependence of the perturbation strength on the specific details of the magnetostatic field produced by such devices.

Before we consider these applications, in this section we will outline some basic aspects of the Hamiltonian theory of almost-integrable systems. We do not intend to present a complete presentation of this vast subject, which can be found at excellent available textbooks [6,44,45,64], but only to focus on the relevant theoretical arguments that justify some of the conclusions we reach on the magnetic field line topology in the presence of a small perturbation. In addition, we shall not use here a specific coordinate system but rather the usual formulation in action-angle variables, that may assume different forms depending if we are dealing with cylindrical or polar toroidal coordinates, representing models for large and moderate aspect ratio, respectively.

Let $H_1 = H_1(J,\vartheta,t)$ be the Hamiltonian corresponding to the non-integrable perturbation. The explicit dependence on t reflects the axisymmetry-breaking nature of the perturbation. Consider ϵ a small quantity representing the perturbation strength. Combining with the unperturbed Hamiltonian $H_0(J)$ (which depends only on J since the system is integrable) we have as a general almost-integrable Hamiltonian system the following expression [64]

$$H(J,\vartheta,t) = H_0(J) + \epsilon H_1(J,\vartheta,t), \quad (29)$$

where $\epsilon \ll 1$.

We can assume, without loss of generality, that the perturbation Hamiltonian is doubly periodic in the variables ϑ and t, since both are either angles or smooth functions of angles. Thus, we can formally expand H_1 in a double Fourier series in these variables and write

$$H(J,\vartheta,t) = H_0(J) + \epsilon\sum_{m=-\infty}^{+\infty}\sum_{n=-\infty}^{+\infty}A_{mn}(J)e^{i(m\vartheta-nt)}, \quad (30)$$

where m and n are the poloidal and toroidal mode numbers, respectively, assuming positive or negative variables. The Fourier coefficients A_{mn} are related to the specific type of perturbation we deal with.

A. Magnetic islands

The first theoretical tool we have at hand for investigating the symmetry-breaking effects on the integrable magnetic field line structure is canonical perturbation theory. Its general idea is to find a canonical transformation from the "old" action-angle variables (J,ϑ) to the "new" variables (J',ϑ') in such a way that the new Hamiltonian is integrable, i.e. $H' = H'(J')$. The unknown variable here is the generating function of such canonical transformation $S = S(J',\vartheta)$ (of the second kind), and formally it is a solution of the corresponding Hamilton-Jacobi equation [64]. We look for approximate solutions of it as a perturbative series for the unknown generating function, which is written as a power series in the small parameter ϵ:

$$S(J',\vartheta) = J'\vartheta + \epsilon S_1 + \epsilon^2 S_2 + \ldots, \quad (31)$$

where the lowest order term is simply an identity transformation, and $S_i(J', \vartheta)$ are functions to be determined.

A key question in the perturbation theory is: does this series converge? Even though $\epsilon \ll 1$ this does not warrant automatic convergence for all values of J' because of the resonances which may be present in the Hamiltonian (29). Resonances occur if the combination $m\vartheta - nt$ is stationary, i.e., if the frequencies $\dot{\vartheta}$ and $\dot{t} = 1$ are commensurate, it turns out that there appear divergent terms in the perturbative series [6]. This is the celebrated "small denominator problem", which plagues perturbation theory [44].

From the above discussion it turns out that resonances occur for rational values of the safety factor of the flux surfaces: $q(J_0) = m/n$, where m and n are coprime integers. For the integrable magnetic field models studied in the previous section we have monotonically increasing forms for $q(J)$, from $q = 1$ at magnetic axis to $q = 5$ at the plasma edge. We can thus choose the most appropriate perturbation in order to excite a particular resonance at a given radial location $r_0 = r_0(J_0)$ within the plasma column. This is the basic theoretical principle underlying the design of resonant helical windings (RHW) and ergodic magnetic limiters (EML).

Typically, the presence of resonances changes the topology of flux surfaces wherever they occur in the plasma. Unperturbed flux surfaces have the topology of nested tori, but when a perturbation is switched on, some of these surfaces will survive while others are destroyed, leaving in their place tubular shaped structures called *magnetic islands*. The cross-section of these tubular magnetic islands have the same Hamiltonian structure of a nonlinear pendulum.

In order to obtain physically sound results using perturbation theory we have to remove the resonances, according the secular perturbation theory. The outcome of this calculation is worth the effort, however, since it gives the position and size of the magnetic islands appearing due to the resonances between the equilibrium and perturbing fields. The resonance located at the action $J = J_0$ can be removed by going to a rotating frame through a canonical transformation to new variables, which we usually call "slow" and "fast", due to the difference in their frequencies. The method proceeds by averaging over the "fast" variable, in such a way that we obtain the pendulum Hamiltonian [6]

$$H_{pend} \approx \frac{G}{2}\mathbf{p}^2 - F\cos\mathbf{q}, \tag{32}$$

where $(\mathbf{p}, \mathbf{q})$ are canonically conjugate variables related to the original action-angle variables of the problem. The constants

$$G \equiv m^2 \left.\frac{d^2 H_0}{dJ^2}\right|_{J=J_0}, \tag{33}$$

$$F \equiv -A_{mn}(J_0), \tag{34}$$

are related to the details of the equilibrium and perturbing fields, respectively.

The Hamiltonian (32) characterizes the orbit structure near the resonance for which $q(J_0) = m/n$, and it shall be described from now on simply as being a $m:n$ magnetic island. Bounded orbits for this Hamiltonian occur for action values of amplitude equal to the half-width of this island $(\Delta J)_{m/n}$. The island width and frequency at resonance are given, respectively, by

$$\Delta J_{m/n} = 2\left|\frac{F}{G}\right|^{1/2}, \tag{35}$$

$$\omega_0 = |FG|^{1/2}. \tag{36}$$

Usually, monotonic safety factor radial profiles are considered, as those described by Equation (22). In these cases, each resonance creates only one island chain. However, for non-monotonic safety factors a given resonance may create more than one island chain, whose reconnection gives rise to dimerized islands [65,66].

B. Rational and irrational flux surfaces

The fate of the equilibrium flux surfaces, after a perturbation breaks the system integrability, is basically determined by their safety factors. KAM theory predicts that, for those irrational surfaces with safety factors sufficiently far from a rational m/n, the topology is preserved, and the surfaces are only slightly deformed from the unperturbed tori (KAM surfaces) [6]. On a rational surface and within its neighborhood the KAM theorem fails, and we have to resort to the Poincaré-Birkhoff theorem.

Let us first consider the unperturbed Hamiltonian ($\epsilon = 0$), and a Poincaré cross section of the equilibrium flux surfaces, as in Fig. 11, for example. The flux surfaces are invariant circles in the Poincaré surface of section, each of them characterized by a safety factor $q(J)$. If it is a rational surface, then any point on the invariant circle $q(J) = m/n$ is a period-n fixed point of the Poincaré mapping for the magnetic field lines. According to the Poincaré-Birkhoff theorem there exists an even number ($2kn$, with $k = 1, 2, \ldots$) of fixed points that remain after the perturbation. Half of them are elliptic (linearly stable), with closed trajectories encircling them, and the other half are hyperbolic (linearly unstable). Successive hyperbolic points are connected by a separatrix, repeating the pendulum Hamiltonian pattern. In other words, rational surfaces disappear under the perturbation leaving an even number of fixed points, around which there exists an island chain [67].

The width and frequency related to these islands can be obtained perturbatively, as described in the previous subsection. There is a crucial difference, however,

since for a pendulum the separatrices smoothly join adjacent hyperbolic points, and for a near-integrable system (small ϵ) this is no longer true. The unstable manifold leaving one hyperbolic point intersects the stable manifold arriving at the neighboring hyperbolic point (homoclinic or heteroclinic intersections, depending on whether the crossing manifolds come from the same point or from different points, respectively). If a single intersection occurs, there are an infinite number of such intersections, leading to a sequence of homoclinic points. Since the areas enclosed by the intersections are mapped one into another, these areas are preserved and as successive crossings become closer to a hyperbolic fixed point, the unstable and stable manifolds have to oscillate more wildly.

The region near the separatrix, where the homoclinic or heteroclinic points are abundant, is characterized by the absence of KAM surfaces and consequently chaotic motion, in the sense that the largest Lyapunov exponent is positive and the magnetic field line is no longer constrained to a magnetic surface but can fill some region of nonzero volume [8]. For sufficiently small perturbations, however, this chaotic behavior occurs in regions bounded by KAM surfaces, that act as dikes, preventing large-scale chaotic diffusion. These regions of local separatrix chaos grow as the perturbation amplitude increases. A barrier transition to global field line chaos is usually expected if this amplitude exceeds a critical value [6].

The grounds for the onset of global or large-scale chaos have already been investigated in depth for one-and-a-half degree of freedom near-integrable systems. Rather sophisticated methods, as the renormalization scheme of Escande and Doveil [68], or the Greene's residue technique [69], can determine with great accuracy the threshold for destruction of the last KAM surface between two neighbor resonances. Good results (within the numerical accuracy) can be obtained by using more simple methods, as the modified Chirikov criterion [6]. In its original version, this criterion prescribes the touching of neighbor separatrices in order to achieve global Hamiltonian chaos [70].

When looking for the onset of large-scale field line chaos in the region between the adjacent island chains $m:n$ and $m':n'$, it is useful to work with the so-called *stochasticity parameter* [70]

$$\chi = \frac{(\Delta J)_{m/n} + (\Delta J)_{m'/n'}}{|J_{0m/n} - J_{0m'/n'}|} \qquad (37)$$

where $\Delta J_{m/n}$ is the half-width of the island around a $m:n$ resonance, and $J_{0m/n}$ is the location (in the action space) of the corresponding rational flux surfaces.

The threshold condition for simple island overlap can be written as $\chi_{crit} = 1$. However, this condition turns out to be an overestimation of the necessary perturbation strength, since the locally chaotic regions overlap long before the separatrices themselves. The reasons for this are basically: (a) the finite width of the locally chaotic regions related to each island, taken separately (the separatrix is no longer defined for these islands); (b) there are a multitude of higher-order satellite islands between the overlapping islands, each with their own locally chaotic regions, which also contribute to the process.

Hence, empirical rules, as the "two-thirds" rule ($\chi_{crit} = 2/3$), have been proposed in order to take this fact into account without modifying the simple form of the Chirikov criterion [6]. This simple rule comes from the comparison between the numerically determined value for the onset of large-scale Hamiltonian chaos for the standard (or Chirikov-Taylor) map, and the corresponding prediction, based on the stochasticity parameter (37) [6]. However, it turns out that even this rule is not always a useful tool, since it holds for pairs of islands of similar widths (as is indeed the case for the standard map), which is no longer valid for the perturbation produced by an ergodic limiter for example, that makes islands thinner as we depart from the tokamak periphery. A "four-fifths" rule has then been proposed as a description for some situations in which the overlapping islands are not of comparable widths [71,72].

There is a universal relation between the critical value of the Chirikov parameter (37) to the safety factor q_e in the center of an island: $\chi_{crit} = 4/q_e$. It is universal in the sense that it holds for resonances of arbitrary higher order. The critical value for the limiter current we have just estimated corresponds to the appearance of a chain of five secondary islands, for which $q_e = 5/1$, in the midst of the primary island.

V Resonant Helical Windings

It has been conjectured that disruptive instabilities may result from topological changes in the magnetic surface with safety factor $q = m/n = 2/1$ [30]. A RHW may be used to produce a resonant external perturbation with suitably chosen mode numbers, in order to investigate the onset of this instability and how it could be controlled. The use of RHW with other mode numbers has experimentally shown to help controlling topological changes on other rational magnetic surfaces, like those with $q = 3/2$ [28] and $q = 4/1$ [29].

After the rather general approach to the almost-integrable fields developed in the previous section, we shall apply these concepts in the analysis of the confined plasma under the influence of resonant helical windings (RHW). Just like we have done for the integrable

case, the treatment will be separated for local and polar toroidal coordinates.

A. RHW in local coordinates

Resonant helical windings are m pairs of fila- tary helical conductors, carrying a current I_H i posite directions for adjacent wires, and wound ar the tokamak outer wall ($r = b$) such that the vari

$$u = m\theta - n\varphi$$

has a constant value [see Fig. 13]. This means tha conductors close on themselves after n turns alon poloidal direction, and m turns along the toroidal We will choose the integers m and n so as to exc main resonance at the desired position of a rationa surface with $q = m/n$.

Let us first derive the magnetic field generate such a configuration of RHW. Neglecting both plasma response and the penetration time of the m lic wall we can assume that the magnetic field of a I is a vacuum field, given by $\mathbf{B}_1 = \nabla\Phi_M$, where Φ_M is a magnetic scalar potential satisfying Laplace's equation $\nabla^2\Phi_M(r,\theta,\varphi = 0)$, with proper boundary conditions at $r = b$. Its solution, for $r < b$, is given by [54]

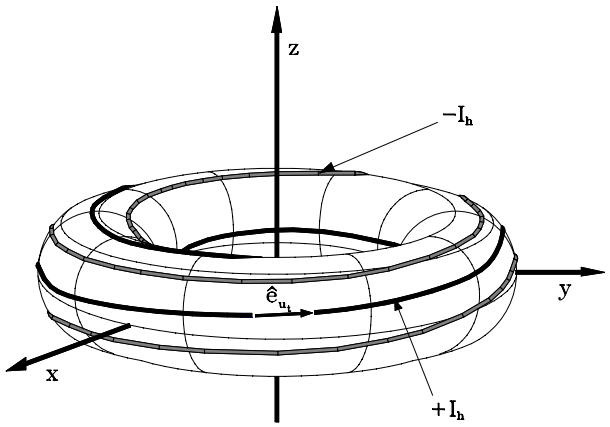

Figure 13. Schematic view of resonant helical windings with $(m, n) = (4, 1)$ in a tokamak.

$$\Phi_M(r,\theta,\varphi) = -\frac{\mu_0 I_H}{\pi}\sum_{p=0}^{\infty}\frac{1}{2p+1}\left(\frac{r}{b}\right)^{m(2p+1)}\sin[(2p+1)(m\theta - n\varphi)], \tag{39}$$

where the magnitude of the terms in this summation decreases very fast with p, such that it suffices to retain only the lowest order term in the above expression ($p = 0$).

Now we derive the explicit form of the perturbation Hamiltonian for a RHW in local coordinates. It should be pointed out, however, that a single RHW does not break the symmetry of the equilibrium configuration. This occurs because, although the time-like variable t appear explicitly in the perturbing magnetic field (39), it does so through the combination expressed by Eq. (38). As a result, we pass from azimuthal to helical symmetry, and a single RHW with cylindrical equilibrium is still an integrable system [73,74].

A way to break the system integrability without adding more RHW is to consider the toroidal correction on the toroidal equilibrium field B_0, given by Eq. (5). This will introduce an additional Fourier series in the perturbation Hamiltonian (30), such that it is rewritten as [57]

$$H_1(J,\theta,\varphi) = \sum_{k,m,n}\left(-\frac{\sqrt{2J}}{R_0}\right)^{|k|}A_{mnk}(J)e^{i(m+k)\theta}e^{-in\varphi}, \tag{40}$$

whose Fourier coefficients are related to the coefficients of the radial perturbing field component $b_{rmn}(J)$ by

$$A_{mnk}(J) = -\frac{\sqrt{2J}R_0 b_{rmn}(J)}{i(m+k)B_0}. \tag{41}$$

For the magnetic scalar potential in (39), it turns out that this coefficient is given by

$$b_{rmn}(r) = i\frac{\mu_0 I_H}{\pi b}\left(\frac{r}{b}\right)^{m-1}. \tag{42}$$

A RHW with mode numbers (m, n) will excite an infinite number of rational surfaces, as result of the

Poincaré-Birkhoff theorem. However, the dominant resonance (in terms of its spectral power) that is excited by such a RHW is the one with $q = m/n$. Using the methods outlined in the previous section we can obtain the width of the $m : n$ island and the frequency at the exact resonance by using Eq. (30), where the constants should be replaced for

$$G \rightarrow \frac{1}{2\pi}(m \pm 1)^2 \left.\frac{d\iota}{dJ}\right|_{J_0}, \tag{43}$$

$$F \rightarrow \frac{\sqrt{2J_0}}{R_0} A_{mn,\pm 1}(J_0), \tag{44}$$

where $J_0 = r_0^2/2$ is given by solving numerically the equation $q(r_0) = m/n$.

Let us present some results of numerical integration of the magnetic field line equations obtained from the equilibrium and perturbing fields in local coordinates with toroidal correction (5). We choose a RHW with $m = 3, n = 1$ because the main resonance to be excited is to be centered at $\approx 0.06m$ inside the plasma (see Fig. 14). The field lines are traced through many turns about the torus from a series of initial conditions. A Poincaré surface of section at $\varphi = 0$ is used to show cross-sections of the field line flow. Fig. 14 shows the phase portrait for a helical current of I_H equal to 0.9% of the plasma current I_P. We see the formation of a main chain of $m = 3$ island related to a mode number 3 : 1. Due to the toroidal correction, the satellite islands 4 : 1 and 2 : 1 have an enhanced appearance. The locations and widths of these islands are in good agreement with the theoretical values [58].

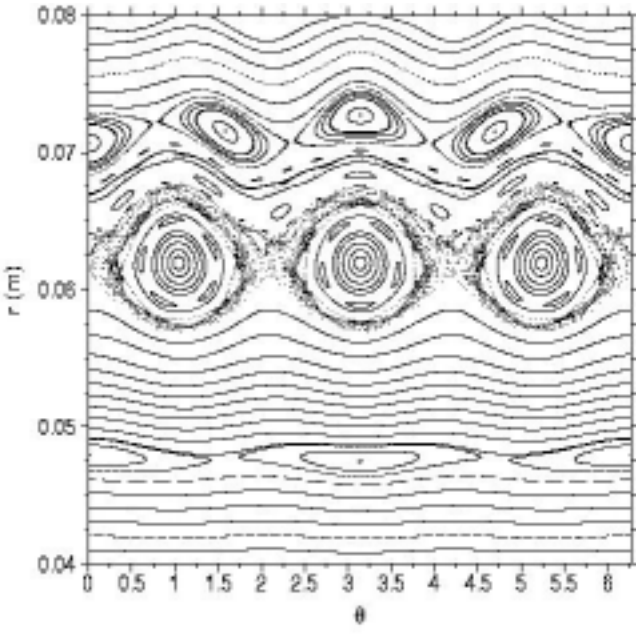

Figure 14. Phase portrait of a Poincaré surface of section map in local coordinates. We consider a RHW with $(m, n) = (3, 1)$ and $I_H = 90A$. The remaining parameters are taken from Table I.

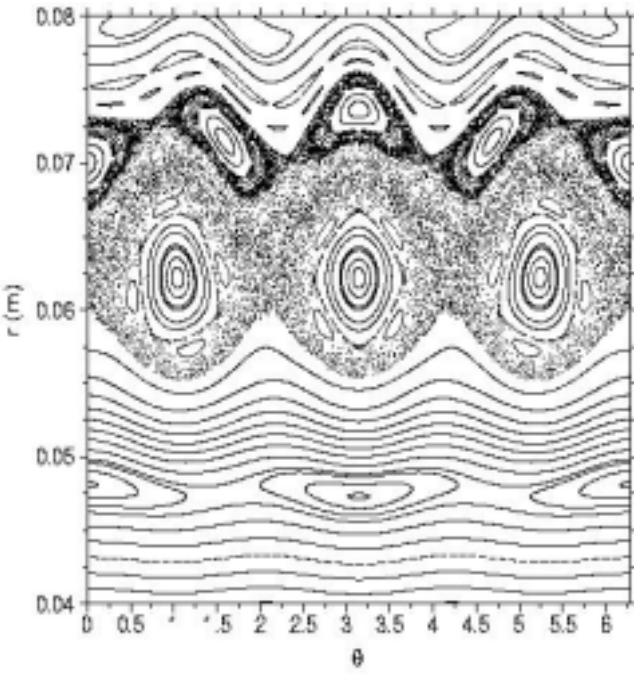

Figure 15. Phase portrait of a Poincaré surface of section map in local coordinates. We consider a RHW with $(m, n) = (3, 1)$ and $I_H = 160A$. The remaining parameters are taken from Table I.

Notice that the main island has a quite sizeable stochastic layer, but there are some remaining magnetic surfaces isolating it from their satellites. In this case, we can see that a thick stochastic layer is formed around the main 3 : 1 island, through interaction of $\ell = 6$ and 7 second-order resonances, since the $\ell = 5$ chain is still visible. Only for higher currents (with I_H equal to 1.6% of I_P, see Fig. 15) we can see the onset of global stochasticity since the 3 : 1 and 4 : 1 island layers interconnect themselves, i.e., field lines wander ergodically through a region comprising both resonances. We also see that the helical current needed to obtain global stochasticity for the 3 : 1-2 : 1 island pair is very large compared with the pair formed with the other satellite, so there is little interest in considering this possibility as the main cause of stochasticity due to this RHW.

For main and satellite islands the amplitude increases with $I_H^{1/2}$, but the toroidal correction introduces a factor proportional to $(r_0/R_0)^{m/2}$ which decreases substantially the satellite half-widths when compared with the main island. The onset of magnetic field line stochasticity between the main island and either of its satellites is described by analyzing the stochasticity parameter (37). Numerical observations of the islands behavior near the transition has pointed that $\chi_{crit} \approx 4/5$ ("four-fifths rule"). It indicates a critical helical current of about 1.4% of the plasma current, considering the overlapping of the 3 : 1-4 : 1 island pair and 2.6% for the pair containing the 2 : 1 satellite, as we have mentioned before.

B. RHW in polar toroidal coordinates

There are many reasons to consider the problem of a RHW that excites mode numbers $m:n$ using a more sophisticated coordinate system, like the polar toroidal (r_t, θ_t, φ): (i) the toroidicity effects are naturally included in the geometry, and there is no need for an *ad hoc* toroidal correction, as for local coordinates; (ii) a realistic design of a RHW needs to take into account the effects of the toroidal geometry. While in a cylindrical approximation the helical pitch is constant, with the effect of toroidicity we find that the pitch is no longer uniform due to the behavior of the toroidal field component, which is stronger in the inner part of the torus.

Hence we use a winding law to best emulate the actual paths followed by magnetic field lines, introducing a tunable parameter λ, such that the variable

$$u_t = m(\theta_t + \lambda \sin\theta_t) - n\varphi_t \tag{45}$$

is constant along a given helical winding [59]. The parameter λ is chosen according to the canonical angle variable ϑ defined in (25). In this section we consider a pair of RHW, located at $u_t = 0$ and $u_t = \pi$, respectively.

We can obtain analytically the magnetic field generated by a RHW in polar toroidal coordinates, by solving the Laplace equation for the magnetic scalar potential. The algebraic manipulations, however, are more involved than the case of local coordinates, and we refer to a previous paper [62] for details of the calculations. The corresponding vector potential $\mathbf{A}_1$, such that $\mathbf{B}_1 = \nabla \times \mathbf{A}_1$ has the covariant component, in lowest order, given by

$$A_{13}(r_t, \theta_t, \varphi) = -\frac{\mu_0 I_H R_0'}{\pi} \sum_{k=-m}^{+m} \mathcal{J}_k(m\lambda) \left(\frac{r_t}{b_t}\right)^{m+k} e^{i[(m+k)\theta_t - n\varphi_t]}, \tag{46}$$

where $\mathcal{J}$ is the Bessel function of order k, and from which the components of the RHW field are given by

$$B_1^1 = -\frac{1}{R_0' r_t}\frac{\partial A_{13}}{\partial \theta_t}, \tag{47}$$

$$B_1^2 = \frac{1}{R_0' r_t}\frac{\partial A_{13}}{\partial r_t}, \tag{48}$$

$$B_1^3 = 0, \tag{49}$$

in which we retained first order powers of the inverse aspect ratio. Notice however that the zeroth order term already contains toroidal effects, since r_t depends on both r and θ [see Appendix]. It is useful to compare this result with that obtained in the limit of cylindrical geometry. In this case we neglect the Shafranov shift such that the magnetic axis coincides with the geometric axis ($R'_0 \to R_0$); and the RHW has now a uniform pitch ($\lambda = 0$), so that the helical variable is simply $u_t \to m\theta - n\varphi$.

In Fig. 16 (a) we show a poloidal profile of the radial component of the field generated by a RHW with $(m,n) = (4,1)$, $(I_H/I_P) = 0.003$, $\lambda = 0.4826$ and at a fixed radial position $r_t/a = 0.911$. We note that the poloidal perturbing field B_1^2 in the internal region (low θ_t) is smaller than in the external region due to the effect of the toroidal curvature on the RHW pitch. Fig. 16 (b) shows a radial profile of the poloidally-averaged radial component $< B_1^1 >$, for similar parameters. It falls down rapidly whenever the radius decreases, so that only the plasma edge region is expected to be noticeably affected by the perturbing helical field.

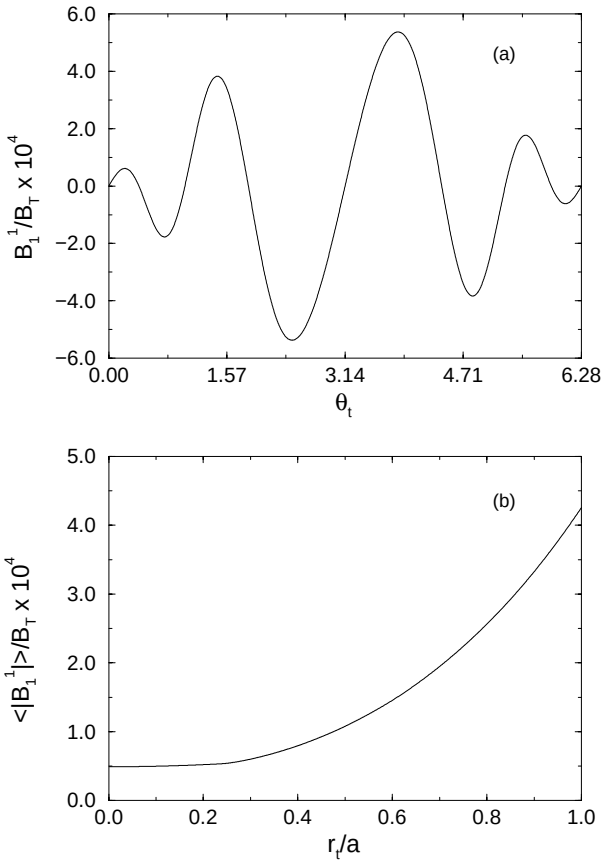

Figure 16. Radial component of the field generated by a $(m,n) = (4,1)$ RHW with $I_H/I_P = 0.003$ and $\lambda = 0.4826$. (a) Poloidal profile for $r_t = 0.91a$; (b) Radial profile for $\theta_t = 5\pi/4$.

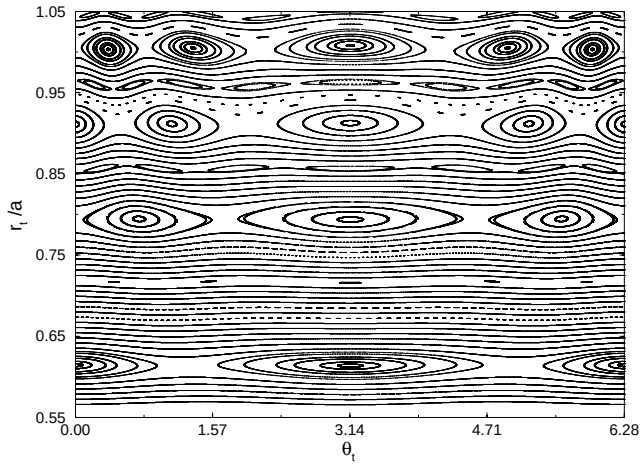

Figure 17. Phase portrait of a Poincaré surface of section map due to a $(4, 1)$ RHW in polar toroidal coordinates, with $I_H/I_P = 0.001$ and $\lambda = 0.4826$. The remaining parameters are taken from Table I.

In Fig. 17 we present a phase portrait of the field line structure due to a $4:1$ RHW in which the current is 0.1% of the total plasma current. The main island to be excited by the RHW is centered at a former magnetic surface with safety factor $q = 4/1$, consistently with the mode numbers here chosen. Other noticeable islands have safety factors $5/1$, $3/1$ and $2/1$, for example. In order to see the effect of the λ parameter on the field line structure, we show in Fig. 18 the same phase portrait, but with $\lambda = 0$. It is apparent that the number of sizeable island chains has been reduced in this case. In particular, the $2:1$ and $3:1$ islands have their widths dramatically decreased. Hence, the use of a winding law such as (45) enhances the resonant effect produced by a RHW.

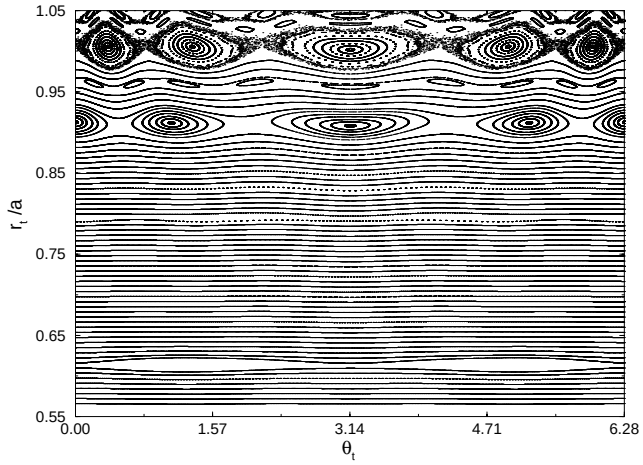

Figure 18. Phase portrait of a Poincaré surface of section map due to a $(4, 1)$ RHW in polar toroidal coordinates, with $I_H/I_P = 0.001$ and $\lambda = 0$.

The RHW current in Fig. 19 has been increased to 0.3% of the total plasma current, and Fig. 20 is the corresponding case for a vanishing λ. We still see many island chains besides the main $4:1$ islands, but there are some differences: (i) the islands' widths have increased; (ii) within the region near to the island separatrix there are thin area-filling portions where the field lines are chaotic. In Fig. 20 we may already see such a region of limited chaotic motion in the neighborhood of the separatrices of the $4:1$ island chain. The other chains have likewise their own chaotic regions, but they are not so evident, either due to their small widths or because the initial conditions used in the phase portrait failed to generate an orbit in the chaotic region.

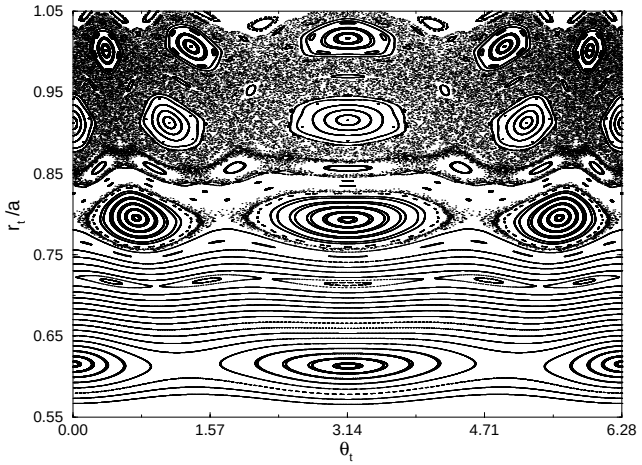

Figure 19. Phase portrait of a Poincaré surface of section map due to a $(4, 1)$ RHW in polar toroidal coordinates with $I_H/I_P = 0.003$ and $\lambda = 0.4826$.

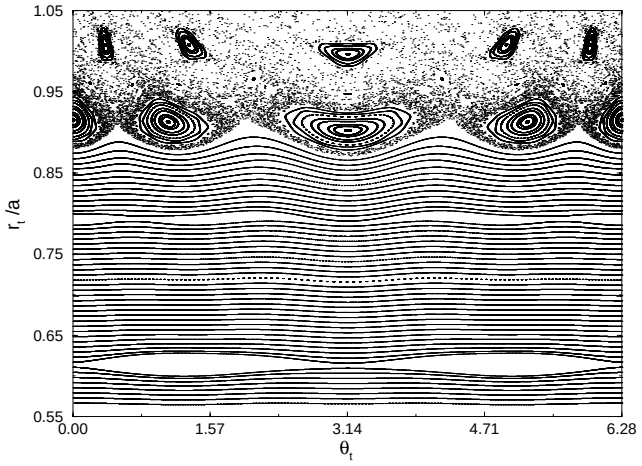

Figure 20. Phase portrait of a Poincaré surface of section map due to a $(4, 1)$ RHW in polar toroidal coordinates with $I_H/I_P = 0.003$ and $\lambda = 0$.

As long as the perturbation is small enough, however, these locally chaotic regions are separated from each other by surviving magnetic surfaces, and the radial excursion of field lines is naturally limited by them. On the other hand, as the perturbation strength increases, the islands' widths also increase, and the

surviving magnetic surfaces are progressively engulfed by locally chaotic regions belonging to adjacent island chains. Depending on the perturbation strength, the adjacent island chains over a given region may be so large that the entire region around them is filled with chaotic field lines. This eventually leads to a globally chaotic region where large-scale chaotic excursions are possible. In the limit of very large perturbation strength, even the elliptic points in the islands' centers may lose their stability and bifurcate, generating other periodic orbits.

VI Ergodic Magnetic Limiters

The non-symmetric character of the magnetic field generated by a RHW is due to the toroidal effect on the helical symmetry. This breaks the integrability (in the Hamiltonian sense) of the equilibrium configuration, thus leading to all the consequences mentioned in the last section, the most important to us being the generation of chaotic field lines. Note that, from the point of view of reducing plasma-wall interactions, it would be useful to create such a chaotic region in the peripheral region of the plasma column.

In principle this is feasible by using a RHW with appropriate values of (m_0, n_0), as the $4:1$ case already studied. However, the mounting of such windings on a tokamak is sometimes a very difficult task, because of the large number of diagnostic windows distributed along the tokamak wall. This has led to the concept of an ergodic magnetic limiter (EML) [23,24], which is composed by one or more grid-shaped current rings of finite length, poloidally wound around the torus. We will consider the EML problem in local and polar toroidal coordinates, in the same spirit we have treated the RHW case.

A. EML in local coordinates

The EML model to be considered here is the same as that originally treated by Martin and Taylor [75,76], but with a different geometry. One EML ring consists of a coil of width ℓ with m pairs of wires oriented in the toroidal direction and carrying a current I_L [Fig. 21]. Adjacent conductors have currents flowing in opposite directions, and we ignore the contributions for the magnetic field from the pieces oriented in the poloidal direction, since their effect on the toroidal field is negligible.

With these simplifications, the EML consists of a bird-cage of $2m$ straight wires equally spaced by an angle π/m. If we were treating wires with "infinite" length (i.e., which extend all over the toroidal circumference $2\pi R_0$, in the periodic cylinder approximation of large aspect ratio) the system would be nothing but a helical winding *without a pitch angle*. Hence, the magnetic field of such a configuration can be obtained from the result derived in the section V.5.

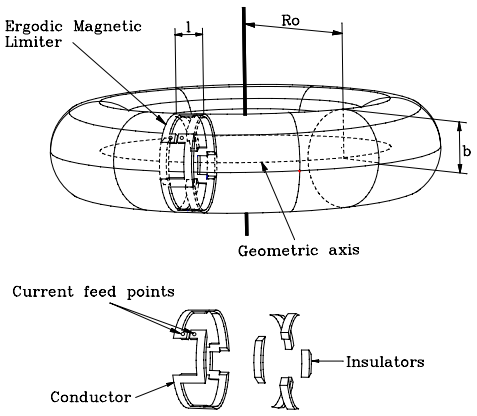

Figure 21. Schematic view of an ergodic magnetic limiter ring. Below: exploded view of one EML ring.

However the wires have finite size ℓ, what breaks the symmetry along the toroidal direction. The absence of favorable boundary conditions turns difficult an analytical solution for the Laplace's equation $\nabla^2\Phi_M = 0$. An *ad hoc* and non-rigorous way of circumventing this problem is to neglect, in a first approximation, the border effects and write the magnetic field generated by an EML in the form $\mathbf{B}_1 = (\tilde{B}_{1r}, \tilde{B}_{1\theta}, 0)$, with the following decomposition [77]

$$B_{1r,\theta}(r,\theta,\varphi) = \tilde{B}_{1r,\theta}(r,\theta) f(\varphi), \tag{50}$$

where $\tilde{B}_{1r,\theta}$ are the magnetic field components of infinitely long wires [78]

$$\tilde{B}_{1r}(r,\theta) = -\frac{\mu_0 m I_L}{\pi b}\left(\frac{r}{b}\right)^{m-1}\sin(m\theta), \tag{51}$$

$$\tilde{B}_{1\theta}(r,\theta) = -\frac{\mu_0 m I_L}{\pi b}\left(\frac{r}{b}\right)^{m-1}\cos(m\theta). \tag{52}$$

The toroidal dependence of the EML fields is described by the function $f(\varphi)$. Two kinds of functions have been used in our previous work on this subject [77]: (i) square-pulse waveforms

$$f(\varphi) = \begin{cases} 1, & \text{if } -\frac{\ell}{2R_0} \le \varphi \le +\frac{\ell}{2R_0}, \\ 0, & \text{otherwise,} \end{cases} \tag{53}$$

which assumes that the limiter field falls down very sharply out of the ring extension; and (ii) a *Dirac comb*, or a periodic sequence of delta-function kicks

$$f(\varphi) = \frac{\ell}{R_0}\sum_{j=-\infty}^{+\infty}\delta(\varphi - 2\pi j). \tag{54}$$

The way we can see the magnetic field line flow due to an EML depends on what kind of form, from those exposed above, we intend to use. If we adopt a square-wave function, a Poincaré map of field lines can only be obtained by direct numerical integration of the field line equation. However, the use of a periodic sequence of

delta kicks enables us to derive an analytical mapping. The basic idea is that a field line twists freely, according to its rotational transform, until it reaches the limiter at $\varphi = 0, 2\pi, \ldots n\pi$ (for one ring) or $\varphi = 0, 2\pi/p, 4\pi/p, \ldots$ for p rings, when it receives a kick. We define discretized variables r_n and θ_n as the values of the field line coordinates just after the n-th kick.

The map so defined is given by

$$r_{n+1} = r_n - \frac{\xi}{b}\left(\frac{r_n}{b}\right)^{m-1} \sin(m\theta_n^*), \quad (55)$$

$$\theta_{n+1} = \theta_n^* - \frac{\xi}{b^2}\left(\frac{r_n}{b}\right)^{m-2} \cos(m\theta_n^*), \quad (56)$$

where $\xi = \mu_0 m I \ell / B_0 \pi$ measures the strength of the perturbation caused by the EML ring, and

$$\theta_n^* = \theta_n + \frac{2\pi B_\theta(r_n) R_0}{B_0}, \quad (57)$$

in the cylindrical case, and

$$\theta_n^* = 2\arctan[\lambda(r_n)\tan(\Omega(r_n) + \arctan\Xi(r_n,\theta_n))] + 2\pi, \quad (58)$$

with the toroidal correction. The poloidal field in (57) is given in terms of the current profile (4) by applying Ampére's law, and the following auxiliary quantities have been defined:

$$\Omega(r_n) = \frac{\pi R_0 B_\theta(r_n)}{B_0 r_n \Lambda(r_n)}\left(1 - \frac{r_n}{R_0}\right), \quad (59)$$

$$\Lambda(r_n) = \left(1 - \frac{r_n}{R_0}\right)\left(1 - \frac{r_n^2}{R_0^2}\right)^{1/2}, \quad (60)$$

$$\Xi(r_n) = \frac{1}{\Lambda(r_n)}\tan\left(\frac{\theta_n}{2}\right). \quad (61)$$

This map was first derived by Viana and Caldas [79,80], but it is not exactly symplectic (area-preserving) due to the approximations employed in its derivation. This problem, however, was formally overcame by Ullmann and Caldas [81], who have applied a canonical transformation to the variables (r_n, θ_n) with the help of a generating function of the second kind. In this way they have arrived to a radial map which has to be numerically inverted (using Newton's method) to give r_{n+1} in terms of r_n and θ_n.

Numerical results of Poincaré maps have been obtained through the use of the numerical integration (in the square-wave case) and the above analytical map (in the Dirac comb case) [76,77]. In Fig. 22, which was generated using the impulsive excitation map, we show phase portraits for four ($p = 4$) EML rings, each of them with $m = 6$ pairs of wires with length $\ell = 0.08m$. The remaining parameters are taken from Table I, and we present only those results with toroidal correction, and for different limiter currents. We observe many primary island chains, the larger ones corresponding to the $6:1$ resonance, located at $r \approx 0.085m$, followed by $6:2$ islands at $0.060m$, and a series of satellite islands due to the toroidal effect. All these features are in accordance with the theory of quasi-integrable fields developed in the previous section.

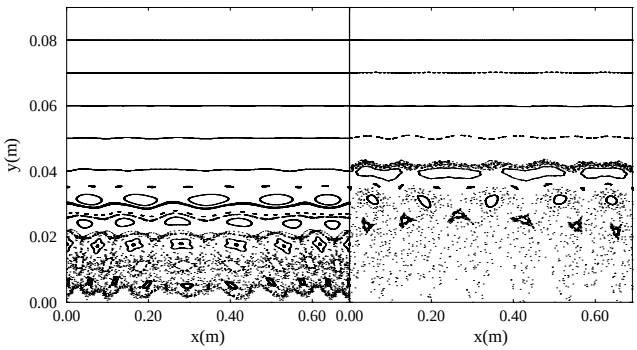

Figure 22. Phase portrait of a Poincaré surface of section map due to a EML with $p = 4$ rings, each of them with $m = 6$ pairs of wires, in the rectangular local coordinates $x = b\theta$ and $y = b - r$. (a) $I_L/I_P = 0.01$; (b) $I_L/I_P = 0.04$.

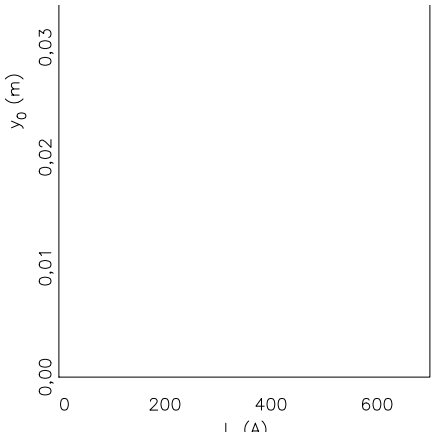

Figure 23. Maximal Lyapunov exponent for a set of initial conditions at $x_0 = 0.60m$ and varying EML current I_L, for the same parameters as in Fig. 22. The Lyapunov exponents are depicted in gray-scale.

An interesting way to analyze the growth of the resonant magnetic island chain and the onset of chaos due to its overlapping with the adjacent ones, as we increase the limiter current, is to compute the maximal Lyapunov exponent for different orbits. In Fig. 23 we plot the leading Lyapunov exponent for various orbits in the Poincaré section, from different initial conditions at different radial positions y_0 and a fixed poloidal angle x_0, and for a varying limiter current I_L. The Lyapunov exponent is represented in gray-scale, and black regions indicate positive values for it. We observe the appearance of the first thin chaotic layers at I_L about 1.0% of I_P, which eventually grow for higher I_L and join other layers to form a large chaotic region [81].

The boundary between chaotic and regular regions in Fig. 23 is quite irregular and actually of a fractal nature. There are light gray tongues entering the borders of the darker chaotic regions corresponding to

secondary island chains which move as we increase I_L. These higher-order islands are eventually destroyed and large-scale chaotic field line flow prevails for large I_L.

B. EML in polar-toroidal coordinates

The analysis outlined in the previous section can be alternatively carried out in polar-toroidal coordinates. The EML consists of N_a slices with length ℓ of a RHW with adequate mode numbers (m_0, n_0), located symmetrically along the toroidal circumference of the tokamak, following a winding law given by (45) (Fig. 21). We shall consider the EML action as a sequence of delta functions at the ring positions. This enables us to obtain a field line mapping, that is derived from a Hamiltonian formulation for the field line flow. Hence the obtained Poincaré map is rigorously area-preserving. The canonical action and angle variables are the same pair $(\mathcal{J}, \vartheta)$ already studied for the RHW case.

The field line Hamiltonian is [62]

$$H(J, \vartheta, t) = H_0(J) + H_1(J, \vartheta, t), \tag{62}$$

where $H_0(J)$ is given by Eq. (24), and

$$H_1(J, \vartheta, t) = \frac{1}{B_T {R_0'}^2} A_{L3}(J, \vartheta, t) \sum_{k=-\infty}^{+\infty} \delta\left(t - k\frac{2\pi}{N_a}\right). \tag{63}$$

The discretized action-angle variables (J_n, ϑ_n) are defined at a n-crossing of a field line with the planes $\varphi_k = t_k = 2\pi k/N_a$, with $k = 0, 1, 2, \ldots N_a - 1$ [77]. Integrating the Hamilton equations corresponding to (62) gives the following mapping for the resulting quasi-integrable system

$$J_{n+1} = J_n - \epsilon\left(\frac{\partial H_1}{\partial \vartheta}\right)(J_{n+1}, \vartheta_n), \tag{64}$$

$$\vartheta_{n+1} = \vartheta_n + \frac{2\pi}{N_a q(J_{n+1})} + \epsilon\left(\frac{\partial H_1}{\partial J}\right)(J_{n+1}, \vartheta_n), \tag{65}$$

where the dimensionless perturbation parameter is defined as

$$\epsilon = \frac{1}{\pi}\left(\frac{\ell}{2\pi R_0'}\right)\left(\frac{I_L}{I_e}\right), \tag{66}$$

and the safety factor $q(J(r_t))$ is given by Eqs. (19) and (20).

Figure 24 shows a phase portrait of the map (64)-(65) for a CML with $N_a = 4$ current rings, each of them being a slice of a RHW with $(m_0, n_0) = (4, 1)$ and $\lambda = 0.4827$, carrying a current of 1.0% of the plasma current I_p. We see a main $4:1$ island chain at $J \approx 0.027$, which corresponds to a normalized radius of $r_t/a \approx 0.9$, such that this chain and its local chaotic region are located near the plasma edge. The CML current has been raised to 1.5% of plasma current in Fig. 25, showing that, for this higher limiter current, the $4:1$ and $5:1$ chains have already partially overlapped, fusing their chaotic regions into a large-scale chaotic layer that extends over a larger peripheral portion of the plasma column. In both cases the chaotic region, although comprising the plasma edge region, does not reach the tokamak wall, due to the existence of many surviving magnetic surfaces in between. If we increase further the limiter current, the chaotic region will become even more pronounced, but it still does not reach the wall. The positive feature of choosing an appropriate $\lambda \neq 0$ is to obtain a chaotic region that is concentrated around a main resonance (the $4:1$ one, in our case), but we observed that for a wide peripheric chaotic region it would be preferable to use $\lambda = 0$ due to the weaker limiter currents required.

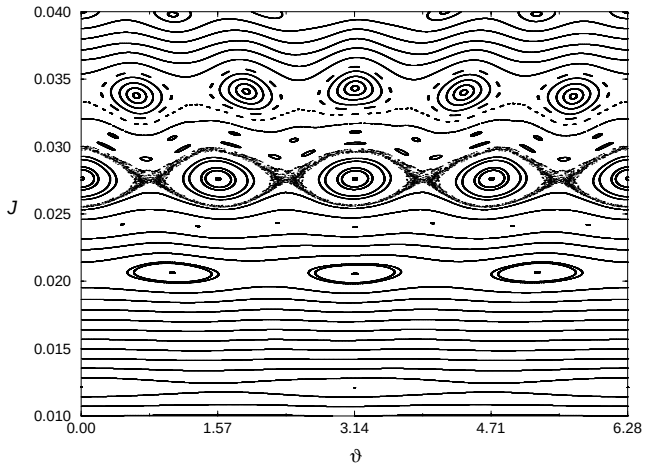

Figure 24. Phase portrait of a Poincaré surface of section map due to a $(4, 1)$ EML in action-angle coordinates with $\lambda = 0.4826$ and $I_L/I_P = 0.010$. The remaining parameters are taken from Table I.

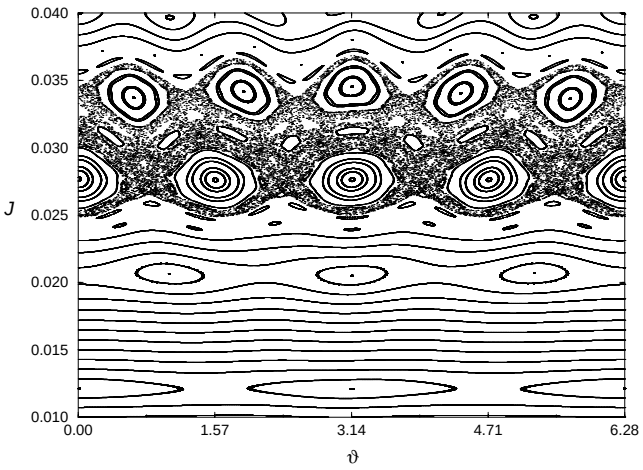

Figure 25. Phase portrait of a Poincaré surface of section map due to a $(4,1)$ EML in action-angle coordinates with $\lambda = 0.4826$ and $I_L/I_P = 0.015$.

Increasing further the limiter current I_L, it may happen that even the centers of the islands - that are stable elliptic fixed points of the limiter mapping - become unstable, and a new set of stable periodic orbits appear. This configures a period-doubling bifurcation, and it is physically related to the creation of new magnetic axes [72].

C. Field line diffusion and loss

One of the advantages of obtaining an analytical mapping is the possibility of tracking many of magnetic field lines by spending a modest computer time, with comparison to the time-consuming task of solving systems of ordinary differential equations for long times. There are numerical studies in which this economy of time makes all the difference. One of them is the computation of the field line diffusion through the peripheral chaotic region generated by a EML.

The quantity of interest here is the average square deviation of the action variable (related to the radial diffusion)

$$< (J - J_0)_n^2 >= \frac{1}{N_\vartheta} \sum_{i=1}^{N_\vartheta} (J_{ni} - J_{0i})^2, \qquad (67)$$

where J_{0i} are different initial conditions, $i = 1, 2, \ldots N_\vartheta$, chosen inside a chaotic region.

This deviation goes asymptotically as n^μ for unbounded diffusion. Anomalous transport is characterized by $\mu \neq 1$, which we name sub-diffusive if $\mu < 1$, and super-diffusive if $\mu > 1$. Gaussian transport is characterized by $\mu = 1$, for which a diffusion coefficient is defined as [82]

$$D_{LF} = \lim_{n\to\infty} \frac{1}{2n} < (J - J_0)_n^2 > . \qquad (68)$$

If the peripheral region were uniformly chaotic we would expect a Gaussian transport. However, since there are many remnants of periodic islands embedded in the chaotic region, the anomalous regime is more likely to be found.

In fact, Fig. 26 shows the results for $< (J - J_0)_n^2 >$ due to a EML for two different limiter currents [83]. We used $N_\vartheta = 4000$ initial conditions picked up from the existent chaotic region and uniformly spread out along the poloidal direction. For the first dozen iterations the transport is super-diffusive due to the strong effect of the positive Lyapunov exponents related to these orbits, and becomes sub-diffusive due to the effect of the periodic islands, that have a trapping effect on the wandering of the field line along the chaotic region. The same features were observed for the Martin-Taylor model for a EML [84].

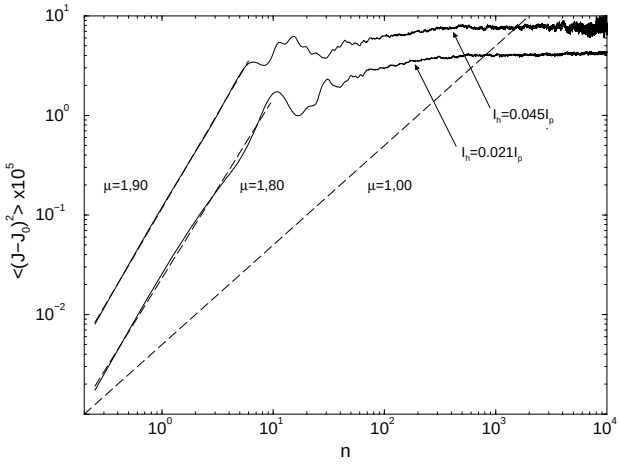

Figure 26. Average square displacement of field lines in the chaotic region due to a $(5,1)$ EML with $\lambda = 0.54$ for two different limiter currents, and n is the number of toroidal turns. The dashed lines correspond to a power law scaling, with the exponents indicated. For comparison, the slope corresponding to the diffusive regime is also shown.

There is a physical limitation for the field line diffusion, however, that is the possibility of a collision between a field line and the wall, after which the field line is considered as lost. This situation is directly related with the problem of heat and particle deposition on the vessel wall. Localized loadings generate high-energy particle impacts that may release impurities adsorbed in the metallic wall, contaminating the plasma. Field line loss leads to a slow decrease of the square deviation for larger times. We found that the decay process is exponential, which can be seen in Fig. 27, where we show the number of lost field lines after n map iterations [83]

$$N_{LF}(n) = N_T \exp\left(-\frac{n - n_0}{\bar{n}}\right), \qquad (69)$$

in which $N_T = 4000$, $n_0 = 69$ and $\bar{n} = 2.39$. This exponential decay possesses actually a staircase fine structure with plateaus with different lengths (see the inset in Fig. 27).

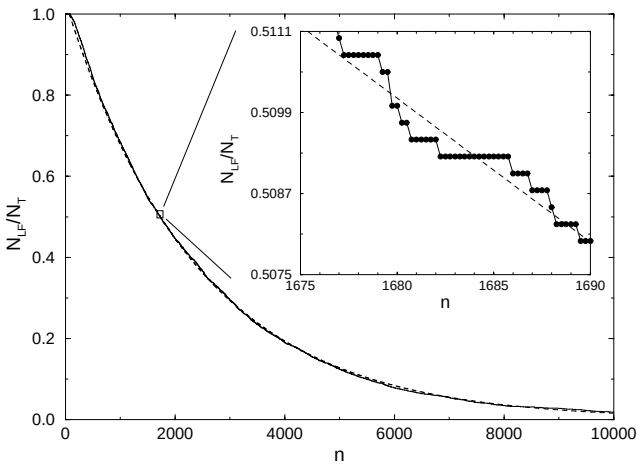

Figure 27. Fraction of field lines that have not collided with the tokamak wall in n map iterations, due to the action of a a $(5,1)$ EML with $\lambda = 0.54$ for $I = 0.045 I_P$. The inset shows the staircase behavior of the exponential decay.

Similarly to a radioactive decay, the statistical process of field line loss is described by two events: a field line hits or does not hit the tokamak wall, and the probability $p_\alpha(m)$ of hitting the wall is much lower than the probability $1-p_\alpha(m)$ of not doing so. This suggests the use of a Poisson probability distribution for the number of observations (each observation corresponds to two toroidal turns) in which m field lines are lost [85]. The validity of this distribution was also confirmed by numerical experiments using our field line map [83].

It is worth mentioning that the chaotic diffusion of field lines is related, but in a rather complicated way, to the particle dynamics within the plasma edge, that we know to be highly turbulent. In the lowest order of approximation, charged plasma particles would be simply advected by the guiding centers of the field lines, but there are many effects related to the finite Larmor radius. For example, the toroidal and poloidal curvatures of field lines lead to curvature drifts, that turn the picture complicated to follow [86]. In spite of these problems, it is possible to estimate the escape time of a charged particle as $\tau_c = 2\pi R_0 < n_c > /v_T$, where $< n_c >$ is the average number of turns a field line takes to collide with the wall, and $v_t = \sqrt{2kT/m}$ is the thermal velocity of impurities with charge eZ_{eff}, where Z_{eff} is the effective atomic number. Our estimates for τ_c suggest that it is less than the total duration of the discharge, making possible for a EML to be used in the impurity control [87]. This estimate, however, does not include the interaction between fast particles (in the tail of the respective velocity distribution) and the wall.

We conclude this section by mentioning that we can regard the action of a EML from a Hamiltonian chaotic scattering point of view. The stable and unstable manifolds of unstable periodic orbits embedded in the peripheral chaotic region play a key role in the non-uniform character of the field line escape process. These manifolds intersect in a very complicated manner, forming a homoclinic tangle which is the underlying dynamical (fractal) structure present in the chaotic field line region [88].

VII Conclusions

Field line chaos, if properly handled, can be of much help in understanding many relevant phenomena in tokamak research, as well as it can help improving the plasma confinement. In this review we have made a comprehensive review of the basic theory underlying chaotic field line formation due to magnetostatic perturbations that breaks system symmetry in tokamaks. We have focused on two specific examples: resonant helical limiters (RHW) and ergodic magnetic limiters (EML). There are many points of contact between the Hamiltonian theory developed for each of them, and some of the experimental findings obtained in tokamaks, with emphasis on the Brazilian TBR-1 tokamak results.

We have seen in Section II that TBR-1 experiments have shown a decrease of MHD activity, i.e., Mirnov oscillations can be damped due to the action of a RHW. Also, a $2:1$ RHW was able to reduce the amplitude of a Mirnov oscillation with the same mode numbers. The theoretical explanation for this fact is that a RHW creates a magnetic island within the plasma that changes the plasma current acting on the rational flux surfaces with safety factor $2/1$ [89]. The Hamiltonian description of field lines and secular perturbation theory reviewed in this paper explain the formation and properties of such an island. We have used two coordinate systems: local and polar-toroidal, which describe situations in which the tokamak aspect ratio is large and moderately large respectively. The positions of such magnetic islands are predicted on the basis of a pre-determined plasma current profile, and it is found that their widths increase with the square-root of the perturbing electric current, what enables us to predict when the resonant $2:1$ chain produced by a RHW will interact with adjacent modes, as the $3:1$ or $4:1$ ones, producing field line chaos. The theoretical results agree with the estimates made on numerical simulations.

Another important experimental result is the cause-effect relationship between minor disruptions and partial island overlap of primary islands. This was verified to occur in TBR-1 for the $2:1$ and $3:1$ islands, and the Poincaré maps for field lines confirm the order of magnitude of the perturbation strength needed for the onset of chaos between these resonances. On the other hand, major disruptions were experimentally shown to be connected with the coupling between the $1:1$ and $2:1$ modes, as detected by soft X-ray analyses. These modes lock their frequencies just before the major disruption occurs.

The physics at the plasma edge seems to be dominated by turbulent particle diffusion, as measured in TBR-1 by means of electrostatic probes. This turbulent diffusion is related, in a non-obvious way, to the chaotic diffusion of field lines in the plasma edge due to an ergodic magnetic limiter (EML). While plasma particles tend to follow magnetic field lines, it turns out that several drifts are also observed which influence the particle flux. Accordingly, the direction of the particle flux is affected by the phase difference between the density and electric potential fluctuations of the drift waves in plasma edge turbulence. This explains the observed flux inversion for some frequency ranges observed in tokamaks.

The expected uniformity of heat and particle loadings on the tokamak wall would be possible only if the chaotic region were uniformly spread out over the poloidal curvature. However, it was experimentally observed a poloidal modulation of these loadings, which is consistent with the anomalous diffusion we have observed numerically, due to the trapping effect of the island remnants. Hence, our diffusion and loss results are more compatible with the actual experimental findings on EML.

From the Hamiltonian point of view, our theoretical framework is essentially based on the KAM theory. Although our description was applied to plasma confinement in tokamaks, we have obtained similar results for other fusion machines, as the reversed field pinch [90]. Further improvements would have to follow other routes, namely to consider the effect of particle diffusion, what needs a drift Hamiltonian formulation [91]. Another technique which could be used to enlighten the relation between field line and particle chaos is the direct numerical integration of particle motion, what is nowadays feasible thanks to many efficient and reliable "particle-in-cell" codes [92]. Kinetic theory treatments are also nowadays being intensively pursued by many research groups for toroidal geometries, due to the demands of neo-classical transport theories [93], and they may shed some new lights on these subjects. As for turbulence theories themselves, there are many attempts to apply the existing theoretical approaches to tokamak situations [40,41,94]. Finally, the model fields treated in this paper were based on realistic geometries and equilibrium profiles, but they are still far from first-principles treatments. However, as far as our investigation was concerned, there is little space to improve further this method in a straightforward way. Future research should be based on techniques of greater sophistication than those here treated.

VIII Appendix

Coordinate systems used in this paper

We briefly describe here the coordinate systems used throughout this paper. A comprehensive source of information about the various existent systems is found in Ref. [95]. A cylindrical system (R, Φ, Z) may be used to describe the tokamak, in which the symmetry (Z-) axis is the major axis of the torus, R is the radial distance from this axis, and Φ is the azimuthal angle (see Fig. 1). The local coordinates (r, θ, φ) are related to these variables by

$$R = R_0 - r\cos\theta, \tag{70}$$
$$Z = \sin\theta, \tag{71}$$
$$\Phi = \varphi. \tag{72}$$

The toroidal coordinates (ξ, ω, φ) are defined as [96]

$$R = \frac{R'_0 \sinh\xi}{\cosh\xi - \cos\omega}, \tag{73}$$
$$Z = \frac{R'_0 \sin\omega}{\cosh\xi - \cos\omega}, \tag{74}$$
$$\Phi = \varphi, \tag{75}$$

in such a way that the coordinate surfaces on which $\xi = const.$ are tori with minor radii $a = R'_0/\sinh\xi$, and major radii $R'_0 \coth\xi$.

The polar toroidal coordinates $(r_t, \theta_t, \varphi_t)$ may be defined in terms of the toroidal coordinates by the following relations [60]

$$r_t = \frac{R'_0}{\cosh\xi - \cos\omega}, \tag{76}$$
$$\theta_t = \pi - \omega, \tag{77}$$
$$\varphi_t = \varphi. \tag{78}$$

The $r_t = const.$ curves have a pronounced curvature in the interior region of the torus, from where we start counting poloidal (θ_t) angles. In Fig. 28 we depict some coordinate surfaces of this system.

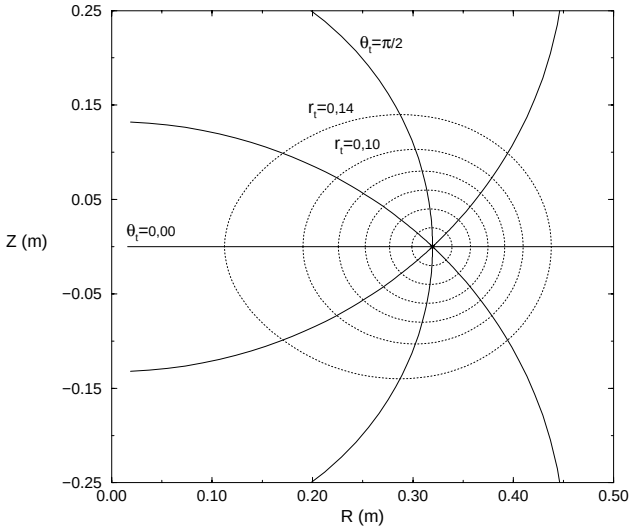

Figure 28. Some coordinate surfaces in the polar toroidal system.

The contravariant basis vectors are

$$\hat{e}^1 = -\frac{r_t}{R'_0}\left(\sinh\xi\hat{e}_\xi + \sin\theta_t\hat{e}_\omega\right), \quad (79)$$

$$\hat{e}^2 = -\frac{1}{r_t}\hat{e}_\omega, \quad (80)$$

$$\hat{e}^3 = -\frac{1}{r_t\sinh\xi}\hat{e}_\xi, \quad (81)$$

where

$$R^2 = R'^2_0\left[1 - 2\left(\frac{r_t}{R'_0}\right)\cos\theta_t - \left(\frac{r_t}{R'_0}\right)^2\sin^2\theta_t\right], \quad (82)$$

The relations between local and polar toroidal coordinates are:

$$r_t = r\left[1 - \left(\frac{r}{R'_0}\right)\cos\theta - \left(\frac{r}{2R'_0}\right)^2\right]^{1/2} \quad (83)$$

$$\sin\theta_t = \sin\theta\left[1 - \left(\frac{r}{R'_0}\right)\cos\theta - \left(\frac{r}{2R'_0}\right)^2\right]^{-1/2} \quad (84)$$

showing that the polar toroidal coordinates tend to the local ones in the large aspect ratio limit ($r \ll R'_0$).

Acknowledgments

This work was made possible with partial financial support of the following agencies: CNPq, CAPES, FAPESP, Fundação Araucária (Paraná), and FUNPAR/UFPR. The authors would like to acknowledge valuable discussions and suggestions from M. Y. Kucinski (IFUSP), H. Tasso, F. Karger, W. Feneberg, F. Lackner (Max-Planck-Institut fuer Plasmaphysik); S. McCool, P. M. Morrison, R. Bengtson (University of Texas at Austin); A. Lichtenberg (University of California at Berkeley), D. Robinson (AEA Fusion, Culham Laboratory, England) and M. Brusati (JET Joint Undertaking, England). We would like to thank S. R. Lopes and I. El Chamaa Neto (UFPR) for helping us with the final version of the manuscript.

References

[1] E. Atlee-Jackson, *Perspectives on Nonlinear Dynamics*, (Cambridge University Press, Cambridge, 1990).

[2] S. J. Camargo, *Turbulence in Fluids and Plasmas*, Publicações IFUSP P-1148 (1995).

[3] A. Yoshizawa, S.-I. Itoh, K. Itoh, and N. Yokoi, *Turbulence Theories and Modeling of Fluids and Plasmas*, National Institute for Fusion Science Research Report NIFS-691, Toki, Japan, April 2001.

[4] X. Chen, P. A. Lindsey, and J. Zhang, Phys. Plasmas **7**, 3976 (2000).

[5] P. Dusenbery, R. F. Martin Jr., and G. R. Burkhart, Chaos **2**, 427 (1992).

[6] A. J. Lichtenberg and M. A. Lieberman, *Regular and Chaotic Dynamics*, 2nd. Edition (Springer-Verlag, Berlin, 1992).

[7] A. J. Dragt and J. M. Finn, J. Geophys. Res. **81**, 2327 (1976).

[8] J.-M. Wersinger, J. M. Finn, and E. Ott, Phys. Fluids **23**, 1142 (1980).

[9] R. Pakter, S. R. Lopes, and R. L. Viana, Physica D **10** , 277 (1997).

[10] J. M. Finn, Nucl. Fus. **15**, 845 (1975.

[11] H. Wobig, Z. Naturforsch. **42a**, 1054 (1987).

[12] A. Bazzani, M. Malavasi, C. Pellacani, S. Siboni, S. Rimbaldi, G. Turchetti, Nuovo Cimento B **103**, 659 (1989).

[13] S. Ortolani, D. D. Schnack, *Magnetohydrodynamics of plasma relaxation* (World Scientific, Singapore, 1993).

[14] J. P. Morrison, Phys. Plasmas **7**, 2279 (2000).

[15] J. Wesson, *Tokamaks* (Oxford University Press, Oxford, 1982).

[16] J. P. Freidberg, *Ideal Magnetohydrodynamics* (Plenum Press, New York, 1987).

[17] R. D. Hazeltine, J. D. Meiss, *Plasma Confinement* (Addison Wesley, 1992).

[18] K. J. Whiteman, Rep. Progr. Phys. **40**, 1033 (1977).

[19] R. Balescu, M. Vlad, and F. Spineanu, Phys. Rev. E **58**, 951 (1998).

[20] S. S. Abdullaev, K. H. Finken, A. Kaleck, and K. H. Spatschek, Phys. Plasmas **5**, 196 (1998).

[21] S. J. Camargo, I. L. Caldas, Plas. Phys. Contr. Fus. **33**, 573 (1991); L. H. A. Monteiro, V. Okano, M. Y. Kucinski, and I. L. Caldas, Phys. Lett. A **193**, 89 (1994).

[22] S. C. McCool et al., Nucl. Fusion **29**, 547 (1989).

[23] F. Karger and F. Lackner, Phys. Lett. A **61**, 385 (1975).

[24] W. Engelhardt and W. Feneberg, J. Nucl. Mat. **76/77**, 518 (1978).

[25] M. S. T. Araujo, A. Vannucci, I. L. Caldas, Nuovo Cim. D **18**, 807 (1996).

[26] A. Grosman et al, Plas. Phys. Contr. Fusion **32**, 1011 (1990); J. C. Vallet *et al.*, Phys. Rev. Lett. **67**, 2662 (1991).

[27] I. H. Tan, I. L. Caldas, I. C. Nascimento, R. P. Silva, E. K. Sanada, and R. Bruha, IEEE Trans. Plasma Sci. **14**, 279 (1986).

[28] D. C. Robinson, Nucl. Fusion **25**, 1101 (1985).

[29] A. Vannucci, I. C. Nascimento, and I. L. Caldas, Plas. Phys. Contr. Fusion **31**, 147 (1989).

[30] Pulsator Team, Nucl. Fusion **25**, 1059 (1985).

[31] A. Vannucci, O. W. Bender, I. L. Caldas, I. C. Nascimento, I. H. Tan, and E. K. Sanada, Nuovo Cim. D **10**, 1193 (1988).

[32] I. C. Nascimento, I. L. Caldas, and R. M. O. Galvão, J. Fus. Energy **12**, 295 (1993).

[33] R. M. O. Galvão et al., Plas. Phys. Contr. Fus. **43**, 1181 (2001).

[34] E. C. da Silva, I. L. Caldas, and R. L. Viana, Braz. J. Phys. **32**, 39 (2002).

[35] A. J. Wootton, B. A. Carreras, H. Matsumoto, K. McGuire, W. A Peebles, Ch. P. Ritz, P. W. Terry, S. J. Sweben, Phys. Plasmas **2**, 2879 (1990).

[36] C. W. Horton, Rev. Mod. Phys. **71**, 735 (1999).

[37] R. P. da Silva, I. C. Nascimento, Rev. Sci. Instruments **62**, 2700 (1991)

[38] M. V. A. P. Heller, R. M. Castro, I. L. Caldas, Z. A. Brasilio, R. P. Silva, I. C. Nascimento, J. Phys. Soc. Japan **66**, 3453 (1997).

[39] M. V. A. P. Heller, Z. A. Brasilio, I. L. Caldas, J. Stöckel, J. Petrzilka, Phys. Plasmas **6**, 846 (1999).

[40] N. Fiedler-Ferrari, C. P. C. do Prado, Plas. Phys. Contr. Fus. **33**, 493 (1991).

[41] M. S. Baptista, I. L. Caldas, M. V. A. P. Heller, A. A. Ferreira, R. D. Bengtson, and J. Stöckel, Phys. Plasmas **8**, 4455 (2001).

[42] I. L. Caldas, M. V. A. P. Heller, R. M. Castro, and E. C. Silva, Physica A **257**, 341 (1998).

[43] M. S. T. Araujo, PhD Thesis, Instituto de Física, Universidade de São Paulo (1997).

[44] A. Osorio de Almeida, *Hamiltonian Systems: Chaos and Quantization* (Cambridge Univ. Press, Cambdridge, 1990).

[45] L. E. Reichl, *The Transition to Chaos* (Springer, Berlin, 1992).

[46] D. W. Kerst, J. Nucl. Energy C **4**, 253 (1962).

[47] N. N. Filonenko, R. Z. Sagdeev, and G. M. Zaslawsky., Nucl. Fusion **7**, 253 (1967).

[48] R. P. Freis, C. W. Hartman, F. M. Hamzeh, and A. J. Lichtenberg, *Nucl. Fusion* **13**, 533 (1973).

[49] F. M. Hamzeh, Nucl. Fusion **14**, 523 (1974).

[50] R. L. Viana, Plas. Phys. Contr. Fusion, **36**, 587 (1994).

[51] R. L. Viana, Braz. J. Phys. **25**, 215 (1995).

[52] R. L. Viana, Tese de Concurso para Professor Titular, Departamento de Física, Universidade Federal do Paraná (1994).

[53] A. S. Fernandes, M. V. A. P. Heller, and I. L. Caldas, Plas. Phys. Contr. Fusion **30**, 1203 (1988).

[54] A. I. Morozov and L. S. Solov'ev, "The structure of magnetic fields," in *Reviews of Plasma Physics*,, vol. 2, Ed. M. A. Leontovich (Consultants Bureau, New York, 1966).

[55] J. M. Greene, Renormalization and the breakup of magnetic surfaces *in:* Statistical physics and chaos in fusion plasmas, Eds. C. P. W. Horton Jr. and L. E. Reichl, (Wiley, New York, 1984).

[56] R. L. Viana, Rev. Mex. Fisica **39**, 902 (1993)

[57] A. J. Lichtenberg, Nucl. Fusion **24**, 1277 (1984).

[58] R. L. Viana, Chaos, Solit. & Fract. **11**, 765 (2000).

[59] X. Y. Yu and J. S. DeGrassie, "Mapping techniques for the GA ergodic magnetic limiter experiment on TEXT," Fusion Research Center, Austin, TX, Univ. Texas Report FRC-292, Nov. 1986.

[60] M. Y. Kucinski and I. L. Caldas, Z. Naturforsch. **42**, 1124 (1987).

[61] M. Y. Kucinski, I. L. Caldas, L. H. A. Monteiro, and V. Okano, J. Plas. Phys. **44**, 303 (1990).

[62] E. C. da Silva, I. L. Caldas, R. L. Viana, IEEE Trans. Plasma Sci. **29**, 617 (2001).

[63] A. Boozer, A. B. Rechester, Phys. Fluids **21**, 682 (1978).

[64] H. Goldstein. *Classical Mechanics* (Addison Wesley, N.Y., 1980).

[65] G. A. Oda, I. L. Caldas, Chaos, Solitons & Fractals **5**, 15 (1995);

[66] G. Corso, G. A. Oda, I. L. Caldas, Chaos, Solitons & Fractals **8**, 1891 (1997).

[67] L. Krlin, Fortsch. Phys. **37**, 735 (1989).

[68] D. F. Escande, Phys. Rep. **121**, 165 (1985).

[69] J. M. Greene, J. Math. Phys. **20**, 1183 (1979).

[70] B. V. Chirikov, Phys. Rep. **52**, 265 (1979).

[71] R. L. Viana and D. B. Vasconcelos, Dynam. Stab. Systems **12**, 75 (1997).

[72] E. C. da Silva, I. L. Caldas and R. L. Viana. Chaos, Solitons & Fractals **14**, 403 (2002).

[73] J. M. Finn, Comments Plas. Phys. Contr. Fus. **14**, 149 (1991).

[74] M. C. R. Andrade, M.Sc. Dissertation, Instituto de Física, Universidade de São Paulo (1989).

[75] T. J. Martin, J. B. Taylor, Plasma Phys. Contr. Fus. **26**, 321 (1984)

[76] N. Reggiani, P. H. Sakanaka, Plas. Phys. Contr. Fus. **36**, 513 (1994).

[77] I. L. Caldas, J. M. Pereira, K. Ullmann, and R. L. Viana, Chaos, Solit. & Fractals **7**, 991 (1996).

[78] R. L. Viana, I. L. Caldas, Eur. J. Phys. **12**, 293 (1991).

[79] R. L. Viana, PhD. Thesis, Instituto de Física, Universidade de São Paulo (1991)

[80] R. L. Viana and I. L. Caldas, Z. Naturforsch. **47**, 941 (1992).

[81] K. Ullmann and I. L. Caldas, Chaos, Solit. & Fract. **11**, 2129 (2000).

[82] J. D. Meiss, Rev. Mod. Phys. **64**, 795 (1992).

[83] E. C. da Silva, I. L. Caldas and R. L. Viana, Phys. Plasmas **8**, 2855 (2001).

[84] J. S. E. Portela, R. L. Viana and I. L. Caldas, Physica A (2002), to be published.

[85] M. G. Bulmer, *Principles of Statistics* (Dover, 1979).

[86] J. A. Bittencourt, *Fundamentals of Plasma Physics*, Second Edition, (FAPESP, São Paulo, 1995).

[87] E. J. da Silva, PhD Thesis, Instituto de Física, Universidade de São Paulo (2001)

[88] E. C. da Silva, I. L. Caldas, R. L. Viana, M. A. F. Sanjuan, Phys. Plasmas (2002) to be published.

[89] I. L. Caldas, H. Tasso, Plas. Phys. Contr. Fusion **20**, 1299 (1978).

[90] L. H. A. Monteiro, M. Y. Kucinski, I. L. Caldas, Plas. Phys. Contr. Fusion **37**, 541 (1995).

[91] W. Horton, H. B. Park, J. M. Kwon, D. Strozzi, P. J. Morrison, and D. I. Choi, Phys. Plasmas **5**, 3910 (1998).

[92] C. K. Birdsall, A. B. Langdom, *Plasma Physics via Computer Simulation* (Adam Hilger, Bristol, 1991).

[93] R. Balescu, Fusion Technology **32**, 192 (1998).

[94] S. J. Camargo, M. K. Tippett, and I. L. Caldas, Phys. Plasmas **7**, 2849 (2000).

[95] W. D. D'haeseleer, W. N. G. Hitchon, J. D. Callen, and J. L. Shohet, *Flux Coordinates and Magnetic Field Structure* (Springer Verlag, Berlin, Heidelberg, New York, 1991).

[96] P. M. Morse and H. Feshbach, *Methods of Theoretical Physics*, (Vol. 2, McGraw Hill, 1953).